J. Fluid Mech. (2011), *vol.* 674, *pp.* 359–388.
doi:10.1017/S0022112010006567

Spheres in the vicinity of a bifurcation: elucidating the Zweifach–Fung effect

V. DOYEUX, T. PODGORSKI, S. PEPONAS, M. ISMAIL AND G. COUPIER†

Université Grenoble 1 / CNRS, Laboratoire Interdisciplinaire de Physique / UMR 5588, Grenoble, F-38041, France

(Received 8 July 2010; revised 26 October 2010; accepted 21 December 2010; first published online 17 March 2011)

The problem of the splitting of a suspension in bifurcating channels divided into two branches of non-equal flow rates is addressed. As has long been observed, in particular in blood flow studies, the volume fraction of particles generally increases in the high-flow-rate branch and decreases in the low-flow-rate branch. In the literature, this phenomenon is sometimes interpreted as the result of some attraction of the particles towards this high-flow-rate branch. In this paper, we focus on the existence of such an attraction through microfluidic experiments and two-dimensional simulations and show clearly that such an attraction does not occur but is, on the contrary, directed towards the low-flow-rate branch. Arguments for this attraction are given and a discussion on the sometimes misleading arguments found in the literature is given. Finally, the enrichment of particles in the high-flow-rate branch is shown to be mainly a consequence of the initial distribution in the inlet branch, which shows necessarily some depletion near the walls.

Key words: blood flow, microfluidics, particle/fluid flows

1. Introduction

When a suspension of particles reaches an asymmetric bifurcation, it is well-known that the particle volume fractions in the two daughter branches are not equal; basically, for branches of comparable geometrical characteristics, but receiving different flow rates, the volume fraction of particles increases in the high-flow-rate branch. This phenomenon, sometimes called the Zweifach–Fung effect (see Svanes & Zweifach 1968; Fung 1973), has been observed for a long time in the blood circulation. Under standard physiological circumstances, a branch receiving typically one fourth of the blood inflow will see its haematocrit (volume fraction of red blood cells) drop down to zero, which will have obvious physiological consequences. The expression 'attraction towards the high-flow-rate branch' is sometimes used in the literature as a synonym for this phenomenon. Indeed, the partitioning not only depends on the interactions between the flow and the particles, which are quite complex in such a geometry, but also on the initial distribution of particles.

Apart from the huge number of *in vivo* studies on blood flow (see Pries, Secomb & Gaethgens 1996 for a review), many other papers have been devoted to this effect, either to understand it, or to use it in order to design sorting or purification devices.

† Email address for correspondence: gwennou.coupier@ujf-grenoble.fr

In the latter case, one can play at will with the different parameters characterizing the bifurcation (widths of the channels and relative angles of the branches), in order to reach a maximum efficiency. As proposed in many papers, focusing on rigid spheres has already given some keys to understand or control this phenomenon (see Bugliarello & Hsiao 1964; Chien *et al.* 1985; Audet & Olbricht 1987; Ditchfield & Olbricht 1996; Roberts & Olbricht 2003, 2006; Yang, Ündar & Zahn 2006; Barber *et al.* 2008). *In vitro* behaviour of red blood cells has also attracted some attention (see Dellimore, Dunlop & Canham 1983; Fenton, Carr & Cokelet 1985; Carr & Wickham 1990; Yang *et al.* 2006; Jäggi, Sandoz & Effenhauser 2007; Fan *et al.* 2008; Zheng, Liu & Tai 2008). The problem of particle flow through an array of obstacles, which can be considered as somewhat similar, has also been studied recently (see El-Kareh & Secomb 2000; Davis *et al.* 2006; Balvin *et al.* 2009; Frechette & Drazer 2009; Inglis 2009).

All the studies mentioned above have focused on the low-Reynolds-number limit, which is the relevant limit for applicative purposes and the biological systems of interest. Therefore, this limit is also considered throughout this paper.

In most studies, as well as in *in vivo* blood flow studies, which are for historical reasons the main sources of data, the main output is the particle volume fraction in the two daughter branches as a function of the flow rate ratio between them. Such data can be well described by empirical laws that still depend on some *ad hoc* parameters but allow some rough predictions (see Dellimore *et al.* 1983; Fenton *et al.* 1985; Pries *et al.* 1989), which have been exhaustively compared recently (see Guibert, Fonta & Plouraboue 2010).

On the other hand, measuring macroscopic data such as volume fraction does not allow identification of the relevant parameters and effects involved in this phenomenon of asymmetric partitioning.

For a given bifurcation geometry and flow rate ratio between the two outlet branches, the final distribution of the particles can be straightforwardly derived from two sets of data: first, their spatial distribution in the inlet and, second, their trajectories in the vicinity of the bifurcation, starting from all possible initial positions. If the particles follow their underlying unperturbed streamlines (as a sphere would do in a Stokes flow in a straight channel), their final distribution can be easily computed, although particles near the apex of the bifurcation require some specific treatment, since they cannot approach it as closely as their underlying streamline does.

The relevant physical question in this problem is thus to identify the hydrodynamic phenomenon at the bifurcation that would make flowing objects escape from their underlying streamlines and, as a consequence, a large particle would be driven towards one branch while a tiny fluid particle located at the same position would travel to the other branch.

In order to focus on this phenomenon, we need to identify more precisely the other parameters that influence the partitioning, for a given choice of flow rate ratio between the two branches.

(i) *The bifurcation geometry.* Audet & Olbricht (1987) and Roberts & Olbricht (2003) made it clear, for instance, that the partitioning in Y-shaped bifurcations depends strongly on the angles between the two branches (see figure 1*a*). For instance, while the velocity is mainly longitudinal, the effective available cross-section to enter a perpendicular branch is smaller than in the symmetric Y-shaped case. Even in the latter case, the position of the apex of the bifurcation relative to the separation line between the fluids travelling in the two branches might play a role, due to the finite size of the flowing objects.

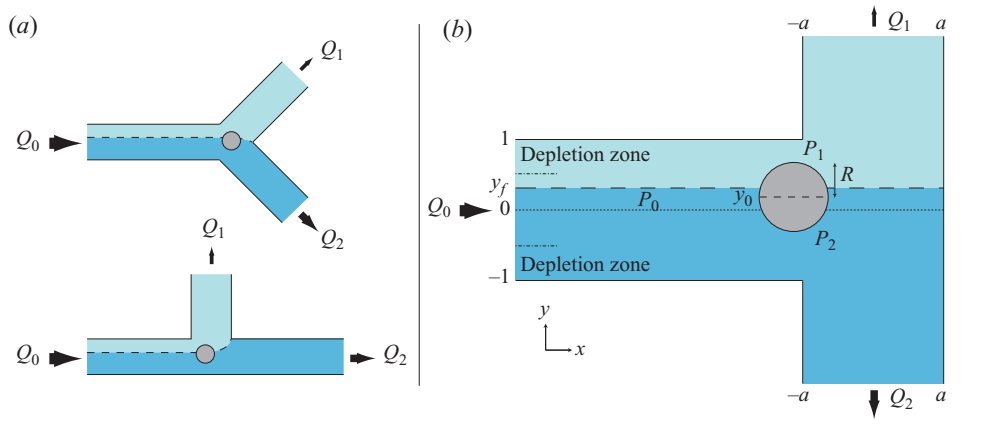

FIGURE 1. (Colour online) (*a*) The two Y-shaped geometries mainly studied in the literature. Here $Q_1 < Q_2$ and the dashed line stands for the separating streamline between the flows that will eventually enter branches 1 and 2 in the absence of particles. (*b*) The T-bifurcation that is studied in this paper and also in Chien *et al.* (1985) in order to remove geometrical effects as much as possible.

(ii) *Radial distribution in the inlet channel.* In an extreme case where all the particles are centred in the inlet channel and follow the underlying fluid streamline, they all enter the high-flow-rate branch; more generally, the existence of a particle free layer near the walls favours the high-flow-rate branch, since the depletion in particles it entails is relatively more important for the low-flow-rate branch, which receives fluid that occupied less space in the inlet branch. The existence of such a particle free layer near the wall has long been observed in blood circulation and is called plasma skimming. More generally, it can be due to lateral migration towards the centre, which can be of inertial origin (high-Reynolds-number regime) (see Schonberg & Hinch 1989; Asmolov 2002; Eloot, De Bisschop & Verdonck 2004; Kim & Yoo 2008; Yoo & Kim 2010) or viscous origin. In such a low-Reynolds-number flow case, while a sphere does not migrate transversally due to symmetry and linearity in the Stokes equation, deformable objects such as vesicles (closed lipid membranes) (see Coupier *et al.* 2008; Kaoui *et al.* 2009), red blood cells (see Bagchi 2007; Secomb, Styp-Rekowska & Pries 2007), which exhibit dynamics similar to vesicles (see Abkarian, Faivre & Viallat 2007; Vlahovska, Podgorski & Misbah 2009), drops (see Mortazavi & Tryggvason 2000; Griggs, Zinchenko & Davis 2007) or elastic capsules (see Risso, Collé-Paillot & Zagzoule 2006; Bagchi 2007; Secomb *et al.* 2007) might adopt a shape that allows lateral migration. This migration is due to the presence of walls (see Olla 1997; Abkarian, Lartigue & Viallat 2002; Callens *et al.* 2008) as well as the non-constant shear rate (see Kaoui *et al.* 2008; Danker, Vlahovska & Misbah 2009). Even in the case where no migration occurs, the initial distribution is still not homogeneous: since the barycentre of particles cannot be closer to the wall than their radius, there is always some particle free layer near the walls. This sole effect will favour the high-flow-rate branch.

(iii) *Interactions between objects.* As illustrated by Ditchfield & Olbricht (1996) or Chesnutt & Marshall (2009), interactions between objects tend to smooth the asymmetry of the distribution, in that the second particle of a couple will tend to travel to the other branch from the first one. A related issue is the study of trains of drops or bubbles at a bifurcation, which completely obstruct the channels and whose

passage in the bifurcation greatly modifies the pressure distribution in its vicinity, and thus influences the behaviour of the following element (see Engl *et al.* 2005; Jousse *et al.* 2006; Schindler & Ajdari 2008; Sessoms *et al.* 2009).

In spite of the large body of literature on this subject, but perhaps because of the applicative purpose of most studies, the relative importance of these different parameters is seldom discussed quantitatively, although most authors are fully aware of the different phenomena at stake.

Since we focus here on the question of cross-streamline migration in the vicinity of the bifurcation, we will consider rigid spheres, for which no transverse migration in the upstream channel is expected. These spheres are in the vanishing concentration limit and flow through symmetric bifurcations, that is the symmetric Y-shaped and T-shaped bifurcations shown in figure 1, where the two daughter branches have the same cross-section and are equally distributed relative to the inlet channel.

Indeed, the case of rigid spheres is still quite unclear in the literature. In the following, first we briefly review previous studies that consider a geometrically symmetric situation and thoroughly re-analyse their results in order to determine whether the Zweifach–Fung effect they see is due to initial distribution or due to some attraction in the vicinity of the bifurcation, which generally has not been done (§ 2).

Then, we present in §§ 3 and 4 our two-dimensional simulations and quasi-two-dimensional experiments (in the sense that the movement of three-dimensional objects is planar). We mainly focus on the T-shaped bifurcation, in order to avoid as much as possible the geometric constraint due to the presence of an apex.

Our main result is that there is some attraction towards the low-flow-rate branch (§ 4.1). This result is then analysed and explained through basic fluid mechanics arguments, which are compared with those previously discussed in the literature.

Secondly, we discuss consequences of this drift on the final distribution in the daughter branches. To do so, we focus on particle concentrations possible at the outlets in the simplest case, where particles are homogeneously distributed in the inlet channel, with the sole (and unavoidable) constraint that they cannot approach the walls closer than their radius (termed *depletion effect* below, see figure 1*b*). This has been done through simulations, which allow us to easily control the initial distribution in particles (§ 4.2). Consequences for the potential efficiency of sorting or purification devices are discussed. We finally recall, in § 4.3, some previous studies from the literature for quantitative comparisons to check the consistency between them and our results.

Before discussing the results from the literature and presenting our data, we introduce useful common notation (see figure 1*b*).

The half-width of the inlet branch is set as the length scale of the problem. The inlet channel is divided into two branches of width $2a$ (the case $a=1$ is mainly considered here by default, unless otherwise stated) and spheres of radius $R \leqslant 1$. The flow rate at the inlet is denoted by Q_0, and Q_1 and Q_2 are the flow rates at the upper and lower outlets ($Q_0 = Q_1 + Q_2$). In the absence of particles, all the fluid particles situated initially above the line $y = y_f$ eventually enter branch 1. This line is called the (unperturbed) fluid separating streamline. Here y_0 is the initial transverse position of the considered particle long before it reaches the bifurcation ($|y_0| \leqslant 1 - R$). N_1 and N_2 are the numbers of particles entering branches 1 and 2 in unit time, while $N_0 = N_1 + N_2$ have entered the inlet channel. The volume fractions in the branches are $\Phi_i = V N_i / Q_i$, where V is the volume of a particle.

With this notation, we can reformulate our question: if $y_0 = y_f$, does the particle experience a net force in the y-direction (e.g. a pressure difference) that would push

it towards one of the branches, while a fluid particle would remain on the separating streamline (by definition of y_f)? If so, for which position y_0^* does this force vanish, so that the particle follows the streamlines and eventually hits the opposite wall and reaches an (unstable) equilibrium position? If $Q_1 \leqslant Q_2$ and $y_0^* < y_f$, then one will talk about *attraction towards the low-flow-rate branch.*

Following this notation, we have

$$N_1 = \int_{y_0^*}^{1} n(y) u_x^*(y)\, \mathrm{d}y, \tag{1.1}$$

$$Q_1 = \int_{y_f}^{1} u_x(y)\, \mathrm{d}y, \tag{1.2}$$

where $n(y)$ is the mean density of particles at height y in the inlet branch, and u_x^* and u_x are respectively particle and flow longitudinal upstream velocities. Note that N_0 and Q_0 are given by the same formula with $y_0^* = y_f = -1$.

The Zweifach–Fung effect can then be written as follows: if $Q_1/Q_0 < 1/2$ (branch 1 receives less flow than branch 2), then $N_1/N_0 < Q_1/Q_0$ (branch 1 receives even less particles than fluid) or equivalently $\Phi_1 < \Phi_0$ (the particle concentration decreases in the low-flow-rate branch).

2. Previous results in the literature

In the literature, the most common symmetric case that is considered is the Y-shaped bifurcation with daughter branches leaving the bifurcation with a 45° angle relative to the inlet channel, and cross-sections identical as those of the inlet channel (figure 1*a*) (see Audet & Olbricht 1987; Ditchfield & Olbricht 1996; Roberts & Olbricht 2003, 2006; Yang *et al.* 2006; Barber *et al.* 2008). The T-shaped bifurcation (figure 1*b*) has attracted little attention (see Yen & Fung 1978; Chien *et al.* 1985). All studies but Yen & Fung (1978) showed results for rigid spherical particles, while some results for deformable particles are given by Yen & Fung (1978) and Barber *et al.* (2008). Explicit data on a possible attraction towards one branch are scarce and can only be found in a recent paper dealing with two-dimensional simulations (see Barber *et al.* 2008). In three other papers, dealing with two-dimensional simulations (see Audet & Olbricht 1987) or experiments in square cross-sectional channels (see Roberts & Olbricht 2006; Yang *et al.* 2006), the output data are the concentrations Φ_i at the outlets. In this section, we re-analyse their data in order to discuss the possibility of an attraction towards one branch. Experiments in circular cross-sectional channels were also performed (see Yen & Fung 1978; Chien *et al.* 1985; Ditchfield & Olbricht 1996; Roberts & Olbricht 2003), on which we comment later in the text.

In the two-dimensional simulations presented by Audet & Olbricht (1987), some trajectories around the bifurcation are shown; however, the authors focused on an asymmetric Y-shaped bifurcation. In addition, some data for N_1/N_0 in a symmetric Y-shaped bifurcation and $R = 0.5$ are presented. Yang *et al.* (2006) performed experiments with balls of similar size ($R = 0.46$) in a symmetric Y-shaped bifurcation with a square cross-section and showed data for N_1/N_0 as a function of Q_1/Q_0 (see Yang *et al.* 2006). Experiments with larger balls ($R = 0.8$) in square cross-sectional channels were carried out by Roberts & Olbricht (2006). Once again, the output data are the ratios N_1/N_0. In both experiments, the authors made the assumption that the initial ball distribution is homogeneous, as also considered in a paper on simulation by Audet & Olbricht (1987). In these three papers, although the authors

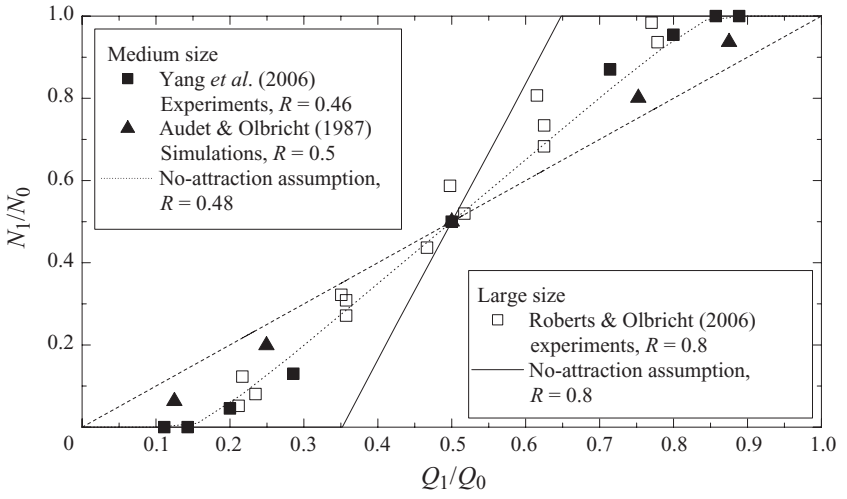

FIGURE 2. Comparison between data from the literature and theoretical distribution under the assumption of no attraction, which would indicate some previously unseen attraction towards the low-flow-rate branch. Rigid spheres distribution N_1/N_0 is shown as a function of the flow distribution Q_1/Q_0 in a symmetric Y-shaped bifurcation and a homogeneous distribution at the inlet (but the unavoidable *depletion effect*). Symbols: data extracted from previous papers: ■, Yang *et al.* (2006, figure 3), experiments, $R = 0.46$; ▲, Audet & Olbricht (1987, figure 8), two-dimensional simulations, $R = 0.5$; □, Roberts & Olbricht (2006, figure 5A), experiments, $R = 0.8$. Dotted and full lines, theoretical distribution for $R = 0.48$ and $R = 0.8$ in the case where the particles follow their underlying streamline ($y_0^* = y_f$: no-attraction assumption) and u_x^* given by our simulations; dashed line, fluid distribution ($N_1/N_0 = Q_1/Q_0$).

were sometimes conscious that the depletion and attraction effects might screen each other, the relative weight of each phenomenon has not been discussed. However, Yang *et al.* (2006) explicitly considered that there must be some *attraction towards the high-flow-rate branch* and gave some qualitative arguments for this. This opinion, initially introduced by Fung (see Fung 1973; Yen & Fung 1978; Fung 1993), is widespread in the literature (see El-Kareh & Secomb 2000; Jäggi *et al.* 2007; Kersaudy-Kerhoas *et al.* 2010). We shall come back to the underlying arguments in the following.

In figure 2, we present the data of N_1/N_0 as a function of Q_1/Q_0 taken from Audet & Olbricht (1987) for $R = 0.5$ (two-dimensional simulations), Yang *et al.* (2006) for $R = 0.46$ (experiments) and Roberts & Olbricht (2006) for $R = 0.8$ (experiments). It is instructive to compare these data with the corresponding values calculated with a very simple model based on the assumption that no particular effect occurs at the bifurcation, that is, the particles follow their underlying streamline (*no-attraction assumption*). To do so, we consider the two-dimensional case of flowing spheres and calculate the corresponding N_1 according to (1.1). The no-attraction assumption implies that $y_0^* = y_f$ and, as in the considered papers, the density $n(y)$ is considered constant for $|y| \leqslant 1 - R$. The particle velocity u_x^* is given by the simulations presented in § 4.2. Since we consider only flow ratios, this two-dimensional approach is a good enough approximation to discuss the results of the three-dimensional experiments, as the fluid separating plane is orthogonal to the plane where the channels lie; moreover, the position of this plane differs only by a few per cent from that of the separating line in two dimensions.

In all curves, it is seen that, if $Q_1/Q_0 < 1/2$, then $N_1/N_0 < Q_1/Q_0$, which is precisely the Zweifach–Fung effect. Note that this effect is present even under the no-attraction

assumption: as already discussed, the sole depletion effect is sufficient to favour the high-flow-rate branch.

Let us first consider spheres of medium size ($R \simeq 0.48$, Audet & Olbricht 1987 and Yang *et al.* 2006). If we compare the data from the literature with the theoretical curve found under the no-attraction assumption, we see that the enrichment of particles in the high-flow-rate branch is less pronounced than in the simulations by Audet & Olbricht (1987) and of the same order in the experiments by Yang *et al.* (2006). Therefore, we can assume that in the two-dimensional simulations by Audet & Olbricht (1987), there is an attraction towards the low-flow-rate branch, which lowers the enrichment of the high-flow-rate branch. The case of the experiments is less clear: it seems that no particular effect takes place.

The $R = 0.8$ case is even more striking: under the no-attraction assumption, we can see that for $Q_1/Q_0 < 0.35$, $N_1 = 0$ because $y_f > 1 - R$ and no sphere can enter the low-flow-rate branch. However, a non-negligible number of particles are found to enter branch 1 for $Q_1/Q_0 < 0.35$ by Roberts & Olbricht (2006) in their experiments (see figure 2). Thus, it is clear that there must be some attraction towards the low-flow-rate branch.

For channels with circular cross-sections, the data found in the literature do not all tell the same story, although spheres of similar sizes are considered. In Chien *et al.* (1985), $R = 0.79$ spheres are considered in a T-shaped bifurcation. The Y-shaped bifurcation was considered twice by the same research group, with very similar spheres: $R = 0.8$ (see Ditchfield & Olbricht 1996) and $R = 0.77$ (see Roberts & Olbricht 2003). In a circular cross-sectional channel, the plane orthogonal to the plane where the channels lie, parallel to the streamlines in the inlet channel and located at distance 0.78 from the inlet channel wall corresponds to the flow-separating plane for $Q_1/Q_0 = 0.32$. At low concentrations, very few spheres are observed in branch 1 for $Q_1/Q_0 < 0.32$ in Chien *et al.* (1985, figure 3D) and Ditchfield & Olbricht (1996, figure 3), in agreement with a no-attraction assumption. Chien *et al.* (1985) also showed that their data can be well described by the theoretical curve calculated by assuming that the particles follow their underlying streamlines. In marked contrast to these results, a considerable number of spheres are still observed in branch 1 in the same situation in Roberts & Olbricht (2003, figure 4). Similarly, in Ditchfield & Olbricht (1996, figure 4), many particles with $R = 0.6$ are found to enter the low-flow-rate branch 1 even when $Q_1/Q_0 < 0.19$, which would indicate some attraction towards the low-flow-rate branch. Thus, in a channel with circular cross-section, the results are contradictory. In the pioneering work of Yen & Fung (1978), a T-shaped bifurcation is also considered, with flexible disks mimicking red blood cells, but the deformability of these objects and the noise in the data do not allow us to make any reasonable comments.

More recently, Barber *et al.* (2008) have presented simulations of two-dimensional spheres with $R \leqslant 0.67$ and two-dimensional deformable objects mimicking red blood cells in a symmetric Y-shaped bifurcation. The values of y_0^* as a function of the flow rate ratios and the spheres radius are clearly discussed. For spheres, it is shown that $y_0^* < y_f$ if $Q_1 < Q_2$, that is, there is an *attraction towards the low-flow-rate branch*, which increases with R. Deformable particles are also considered. However, it is not possible to discuss from their data (or, probably, from any other data) whether the cross-streamline migration at the bifurcation is more important in this case or not: for deformable particles, transverse migration towards the centre occurs due to the presence of walls and non-homogeneous shear rates. This migration will probably screen the attraction effect, at least partly, and it seems difficult to quantify the relative

contribution of both effects. In particular, y_0^* depends on the (arbitrary) initial distance from the bifurcation. In Chesnutt & Marshall (2009), attraction towards the low-flow-rate branch is also quickly evoked, but considered as negligible since the focus was on large channels and interacting particles.

Finally, from our new analysis of previous results from the literature (and despite some discrepancies) it appears that there should be some attraction towards the low-flow-rate branch, although the final result is an enrichment of the high-flow-rate branch due to the depletion effect in the inlet channel. This effect was seen by Barber *et al.* (2008) in their simulations. On the other hand, if one considers the flow around an obstacle, as simulated in El-Kareh & Secomb (2000), it seems that spherical particles are attracted towards the high-flow-rate side.

From the above discussion, we conclude that the different effects occurring at the bifurcation level are neither well identified nor explained. Moreover, to date, no direct experimental proof of any attraction phenomenon exists. In § 4.1, we show experimentally that attraction towards the low-flow-rate branch takes place and confirm this through numerical simulations.

It is then necessary to discuss whether this attraction has important consequences on the final distributions in particles in the two daughter channels. This was not done explicitly in Barber *et al.* (2008); however, in § 4.2 through simulations we discuss the relative weight of the attraction towards the low-flow-rate branch and the depletion effect, which have opposite consequences.

3. Method

3.1. *Experimental set-up*

We studied the behaviour of hard balls as a first reference system. Since the potential migration across streamlines is linked to the way the fluid acts on the particles, we also studied spherical fluid vesicles. These are closed lipid membranes enclosing a Newtonian fluid. The lipids that we used are in liquid phase at room temperature, so that the membrane is a two-dimensional fluid. In particular, it is incompressible (so that spherical vesicles will remain spherical even under stress, unlike drops), but it is easily sheared: this means that a torque exerted by the fluid on the surface of the particle can imply a different response depending on whether it is a solid ball or a vesicle. Moreover, since vesicle suspensions are polydisperse, it is a convenient way to vary the radius R of the studied object.

The experimental set-up is a standard microfluidic chip made of polydimethylsiloxane bonded on a glass plate (figure 3). We wish to observe what happens to an object located around position y_f, that is, in which branch it goes at the bifurcation. In order to determine the corresponding y_0^*, we need to scan different initial positions around y_f. One solution would be to let a suspension flow and hope that some of the particles are close enough to the region of interest. In the meantime, as we shall see, the cross-streamline effect is weak and requires precise measurement, and noticeable effects appear only at high radius R, typically $R > 0.5$. Clogging is unavoidable with such objects, which would modify the flow rates ratio, and if a very dilute suspension is used, it is likely that the region of interest will only partly be scanned.

Therefore, we designed a microfluidic system that allowed us to use only one particle, which would go through the bifurcation with a controlled initial position y_0, would be taken back, its position y_0 modified, would flow again through the bifurcation, and so on. Moreover, we allowed continuous modification of the flow rate ratio between the two daughter branches. The core of the chip is the five branch

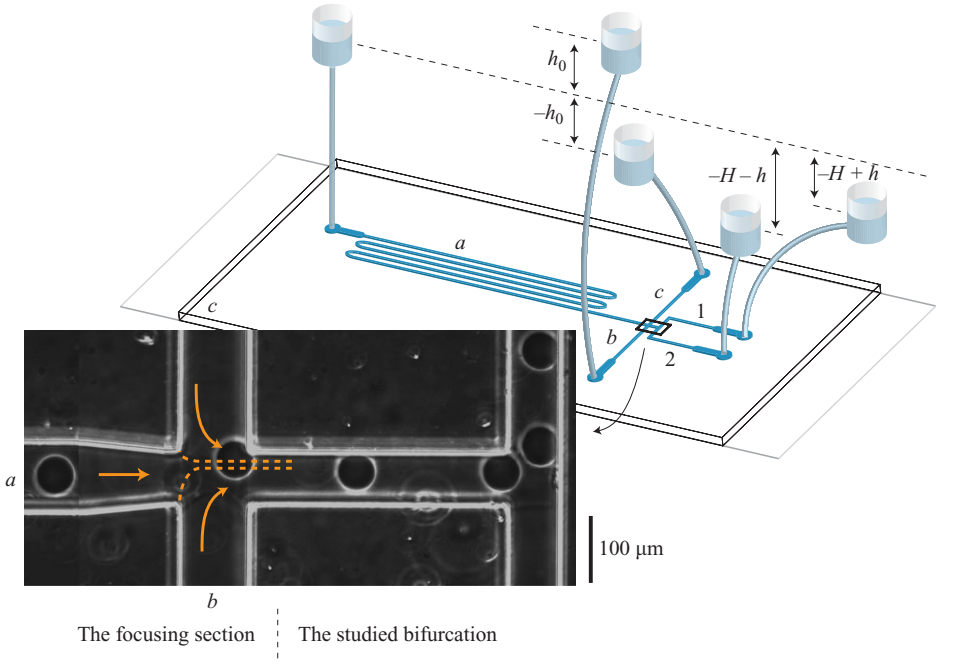

FIGURE 3. (Colour online) Scheme of the microfluidic device. The photograph shows the trajectory of a particle from branch a to branch 1 after having been focused on a given streamline thanks to flows from lateral branches b and c.

crossroad shown in the inset to figure 3. These five branches have different lengths and are linked to reservoirs placed at different heights, in order to induce flow by a hydrostatic pressure gradient. A focusing device (branches a–c) is placed before the bifurcation of interest (branches 1 and 2), in order to control the lateral position of the particle. Particles are initially located in the central branch a, where the flow is weak and the incoming particles are pinched between the two lateral flows. In order to modify the position y_0 of the particle, the relative heights of the reservoirs linked to the lateral branches are modified. The total flow rate and the flow rate ratios between the two daughter branches after the bifurcation are controlled by varying the heights of the two outlet reservoirs. Note that the flow rate ratio also depends on the heights of the reservoirs linked to inlet branches a, b and c. Since the latter two must be continuously modified to vary the position y_0 of the incoming particle in order to find y_0^* for a given flow rate ratio, it is convenient to place them on a pulley so that their mean height is always constant (resistances of branches b and c being equal). If the total flow rate is a relevant parameter (which is not the case here since we consider only Stokes flow of particles that do not deform), one can do the same with the two outlet reservoirs. In such a situation, if the reservoir of branch a is placed at height 0, reservoirs of branches b and c at heights $\pm h_0$, and reservoirs of branches 1 and 2 at heights $-H+h$ and $-H-h$, the flow rate ratio is governed by setting (h, H) and h_0 can be modified independently in order to control y_0. Once the particle has gone through the bifurcation, height H and the height of reservoir a are modified so that the particle comes back to branch a, and h_0 is modified in order to get closer and closer to the position y_0^*. Note that Q_1/Q_0 (or equivalently y_f) is a function of H, h, and the flow resistances of the five branches of rectangular cross-sections, which

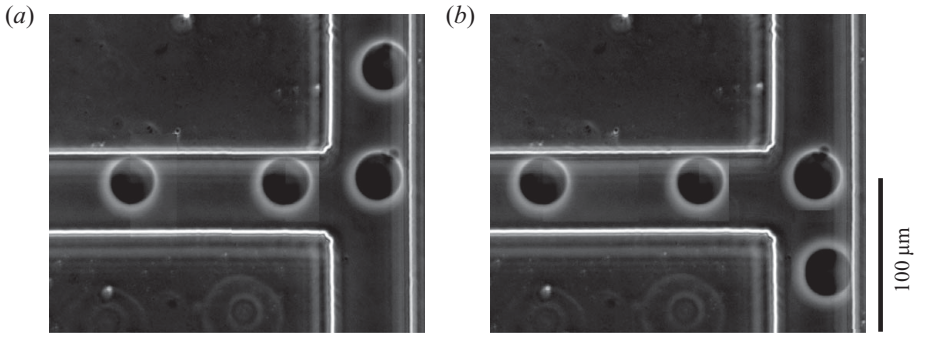

FIGURE 4. Photographs showing the different positions of a vesicle of radius $R = 0.60$ starting just above and just below its separating line. No clear difference between these two starting positions can be seen by eye, which illustrates the accuracy we get in the measurement of y_0^*. Here Q_1/Q_0 is set to 0.28.

are known functions of their lengths, widths and thicknesses (see White 1991). The accuracy of the calculation of this function was checked by measuring y_0^* for small particles, which must be equal to y_f.

Note that the length of the channel is much more important than the size of a single flowing particle, so that we can neglect the contribution of the latter in the resistance to the flow: hence, even though we control the pressures, we can consider that we work at fixed flow rates.

Finally, as can be seen in figure 4, our device allows us to scan very precisely the area of interest around the sought y_0^*, so that the uncertainty associated with it is very low.

At the bifurcation level, channels widths are all equal to $57 \pm 0.2\,\mu$m. Their thickness is $81 \pm 0.3\,\mu$m. We used polystyrene balls of maximum radius $40.5 \pm 0.3\,\mu$m in soapy water (therefore $R \leqslant 0.71$) and fluid vesicles of size $R \leqslant 0.60$. The vesicle membrane is a dioleoylphosphatidylcholine lipid bilayer enclosing an inner solution of sugar (sucrose or glucose) in water. Vesicles are produced following the standard electroformation method (see Angelova *et al.* 1992). Maximum flow velocity at the bifurcation level was around $1\,\text{mm s}^{-1}$, so that the Reynolds number $Re \simeq 10^{-1}$.

3.2. *The numerical model*

In the simulations, we focus on the two-dimensional problem (invariance along the z-axis). Our problem is a simple fluid/structure interaction and can be modelled by Navier–Stokes equations for the fluid flow and Newton–Euler equations for the sphere. These two problems can be coupled in a simple manner.

(i) The action of fluid on the sphere is modelled by the hydrodynamic force and torque acting on its surface. They are used as the right-hand sides of Newton–Euler equations.

(ii) The action of the sphere on fluid can be modelled by no-slip boundary conditions on the sphere (in the Navier–Stokes equations).

However, this explicit coupling can be numerically unstable and its resolution often requires very small time steps. In addition, as we have chosen to use the finite element method (FEM) (for accuracy) and since the position of the sphere evolves in time, we have to remesh the computational domain at each time step or in best cases every few time steps.

For these reasons, we chose another strategy to model our problem. Instead of using Newton–Euler equations for modelling the sphere motion and Navier–Stokes equations for the fluid flow, we use only the Stokes equations in the entire domain of the bifurcation (including the interior of the sphere). The use of Stokes equations is justified by the small Reynolds number in our case and the presence of the sphere is rendered by a second fluid with a 'huge' viscosity on which we impose a rigid body constraint. Such a strategy is widely used in the literature under different names, e.g. the so-called fluid particle dynamics (FPD) method (see Tanaka & Araki 2000; Peyla 2007), but we can group them generically as penalty-like methods. The method used here was mainly developed by Lefebvre *et al.* (see Janela, Lefebvre & Maury 2005; Lefebvre 2007) and we can find a mathematical analysis of such methods in Maury (2009).

In what follows, we briefly describe the basic ingredients of the FEM and the penalty technique applied to the problem.

The fluid flow is governed by Stokes equations written as follows:

$$-\nu\Delta\boldsymbol{u} + \nabla p = 0 \quad \text{in } \Omega_f, \tag{3.1}$$

$$\nabla\cdot\boldsymbol{u} = 0 \quad \text{in } \Omega_f, \tag{3.2}$$

$$\boldsymbol{u} = \boldsymbol{f} \quad \text{on } \partial\Omega_f, \tag{3.3}$$

where the variables

(i) ν, $\boldsymbol{u}$ and p are respectively the viscosity, velocity and pressure fields of the fluid;

(ii) Ω_f is the domain occupied by the fluid; typically $\Omega_f = \Omega\backslash\bar{B}$ if we denote by Ω the whole bifurcation and by B the rigid particle;

(iii) $\partial\Omega_f$ is the border of Ω_f;

(iv) $\boldsymbol{f}$ is some given function for the boundary conditions.

It is known that under some reasonable assumptions the problem (3.1)–(3.3) has a unique solution $(\boldsymbol{u}, p) \in H^1(\Omega_f)^2 \times L^2_0(\Omega_f)$ (see Girault & Raviart 1986). Below, we use the following functional spaces:

$$L^2(\Omega) = \left\{ f : \Omega \to \mathbb{R}; \int_\Omega |f|^2 < +\infty \right\}, \tag{3.4}$$

$$L^2_0(\Omega) = \left\{ f \in L^2(\Omega); \int_\Omega f = 0 \right\}, \tag{3.5}$$

$$H^1(\Omega) = \{ f \in L^2(\Omega); \nabla f \in L^2(\Omega) \}, \tag{3.6}$$

$$H^1_0(\Omega) = \{ f \in H^1(\Omega); f = 0 \text{ on } \partial\Omega \}. \tag{3.7}$$

As we use the FEM for the numerical resolution of the problem (3.1)–(3.3), we need to rewrite this in a variational form (an equivalent formulation of the initial problem). For the sake of simplicity, we start by writing it in a standard way (fluid without sphere), then we modify it using the penalty technique to take into account the presence of the particle. In what follows, we briefly describe these two methods, the standard variational formulation for the Stokes problem and the penalty technique.

3.2.1. *Variational formulation*

First recall the deformation tensor $\boldsymbol{\tau}$, which is useful in what follows

$$\boldsymbol{\tau}(\boldsymbol{u}) = \tfrac{1}{2}\left(\nabla\boldsymbol{u} + (\nabla\boldsymbol{u})^t\right). \tag{3.8}$$

Thanks to the incompressibility constraint $\nabla \cdot \boldsymbol{u} = 0$, we have

$$\Delta \boldsymbol{u} = 2\nabla \cdot \boldsymbol{\tau}(\boldsymbol{u}). \tag{3.9}$$

Hence, the problem (3.1)–(3.3) can be rewritten as follows: find $(\boldsymbol{u}, p) \in H^1(\Omega_f)^2\, L^2_0(\Omega_f)$ such that

$$-2\nu\nabla \cdot \boldsymbol{\tau}(\boldsymbol{u}) + \nabla p = 0 \quad \text{in } \Omega_f, \tag{3.10}$$

$$\nabla \cdot \boldsymbol{u} = 0 \quad \text{in } \Omega_f, \tag{3.11}$$

$$\boldsymbol{u} = \boldsymbol{f} \quad \text{on } \partial\Omega_f. \tag{3.12}$$

By simple calculations (see the Appendix for details) we show that problem (3.10)–(3.12) is equivalent to the following: find $(\boldsymbol{u}, p) \in H^1(\Omega_f)^2 \times L^2_0(\Omega_f)$ such that

$$2\nu \int_{\Omega_f} \boldsymbol{\tau}(\boldsymbol{u}) : \boldsymbol{\tau}(\boldsymbol{v}) - \int_{\Omega_f} p\nabla \cdot \boldsymbol{v} = 0, \quad \forall \boldsymbol{v} \in H^1_0(\Omega_f)^2, \tag{3.13}$$

$$\int_{\Omega_f} q\nabla \cdot \boldsymbol{u} = 0, \quad \forall q \in L^2_0(\Omega_f), \tag{3.14}$$

$$\boldsymbol{u} = \boldsymbol{f} \quad \text{on } \partial\Omega_f, \tag{3.15}$$

where '$:$' denotes the double contraction.

3.2.2. *Penalty method*

We chose to use the penalty strategy in the framework of FEM, described here briefly (see Janela *et al.* 2005 and Lefebvre 2007 for more details).

The first step consists in rewriting the variational formulation (3.13)–(3.15) by replacing the integrals over the real domain occupied by the fluid ($\Omega_f = \Omega \setminus \bar{B}$) by those over the whole domain Ω (including the sphere B). This means that we extend the solution $(\boldsymbol{u}, p)$ to the whole domain Ω. More precisely, by the penalty method we replace the particle by an artificial fluid with huge viscosity. This has been made possible by imposing a rigid-body motion constraint on the fluid that replaces the sphere ($\boldsymbol{\tau}(\boldsymbol{u}) = 0$ in B). Obviously, the divergence-free constraint is also ensured in B.

The problem (3.13)–(3.15) is then modified as follows: find $(\boldsymbol{u}, p) \in H^1(\Omega)^2\, L^2_0(\Omega)$ such that

$$2\nu \int_{\Omega} \boldsymbol{\tau}(\boldsymbol{u}) : \boldsymbol{\tau}(\boldsymbol{v}) + \frac{2}{\varepsilon} \int_B \boldsymbol{\tau}(\boldsymbol{u}) : \boldsymbol{\tau}(\boldsymbol{v}) - \int_{\Omega} p\nabla \cdot \boldsymbol{v} = 0, \quad \forall \boldsymbol{v} \in H^1_0(\Omega)^2, \tag{3.16}$$

$$\int_{\Omega} q\nabla \cdot \boldsymbol{u} = 0, \quad \forall q \in L^2_0(\Omega), \tag{3.17}$$

$$\boldsymbol{u} = \boldsymbol{f} \quad \text{on } \partial\Omega, \tag{3.18}$$

where $\varepsilon \ll 1$ is a given penalty parameter.

Finally, if we denote the time discretization parameter by $t_n = n\delta t$, the velocity and the pressure at time t_n by $(\boldsymbol{u}_n, p_n)$, the velocity of the sphere at time t_n by $\boldsymbol{V}_n$ and its centre position by $\boldsymbol{X}_n$, we can write our algorithm as

$$\boldsymbol{V}_n = \frac{1}{\text{volume}(B)} \int_B \boldsymbol{u}_n, \tag{3.19}$$

$$\boldsymbol{X}_{n+1} = \boldsymbol{X}_n + \delta t\, \boldsymbol{V}_n, \tag{3.20}$$

where $(\boldsymbol{u}_{n+1}, p_{n+1})$ solves

$$2\nu \int_{\Omega} \tau(\boldsymbol{u}_{n+1}) : \boldsymbol{\tau}(\boldsymbol{v}) + \frac{2}{\varepsilon} \int_{B} \tau(\boldsymbol{u}_{n+1}) : \boldsymbol{\tau}(\boldsymbol{v}) - \int_{\Omega} p_{n+1} \nabla \cdot \boldsymbol{v} = 0, \quad \forall \boldsymbol{v} \in H_0^1(\Omega)^2, \tag{3.21}$$

$$\int_{\Omega} q \nabla \cdot \boldsymbol{u}_{n+1} = 0, \quad \forall q \in L_0^2(\Omega), \tag{3.22}$$

$$\boldsymbol{u}_{n+1} = \boldsymbol{f} \quad \text{on } \partial\Omega. \tag{3.23}$$

The implementation of algorithm (3.19)–(3.23) is done with a user-friendly finite element software Freefem++ (see Hecht & Pironneau 2010).

Finally, we consider the bifurcation geometry shown in figure 1(*b*) and impose no-slip boundary conditions on all walls and prescribe parabolic velocity profiles at the inlets and outlets such that, for a given choice of flow rate ratio, $Q_0 = Q_1 + Q_2$. For a given initial position y_0 of the sphere of radius R at the outlet, the full trajectory is calculated until it definitely enters one of the daughter branches. A dichotomy algorithm is used to determine the key position y_0^*. Spheres of radius R up to 0.8 are considered.

Remark 1. *In practice, the penalty technique may deteriorate the pre-conditioning of our underlying linear system. To overcome this problem, one can regularize (3.22) by replacing it with the following:*

$$-\varepsilon_0 \int_{\Omega} p_{n+1} q + \int_{\Omega} q \nabla \cdot \boldsymbol{u}_{n+1} = 0, \quad \forall q \in L_0^2(\Omega), \tag{3.24}$$

where $\varepsilon_0 \ll 1$ *is a given parameter.*

4. Results and discussion

4.1. *The cross-streamline migration*

4.1.1. *The particle-separating streamlines*

In figure 5, we show the position of the particle-separating line y_0^* relative to the position of the fluid-separating line y_f when branch 1 receives less fluid than branch 2 (see figure 1*b*), which is the main result of this paper. For all particles considered, in the simulations or in the experiments, we find that the particle-separating line lies below the fluid-separating line, the upper branch being the low-flow-rate branch. These results clearly indicate an attraction towards the low-flow-rate branch: while a fluid element located below the fluid-separating streamline will enter into the high-flow-rate branch, a solid particle can cross this streamline and enter into the low-flow-rate branch, provided it is not too far away initially. It is also clear that the attraction increases with the sphere radius R.

In particular, in the experiments (figure 5*a*), particles of radius $R \lesssim 0.3$ behave like fluid particles. Note that $R = 0.52$ balls show a slight attraction towards the low-flow-rate branch, while the effect is more marked for big balls of radius $R = 0.71$. Vesicles show a comparable trend and it seems from our data that solid particles or vesicles with fluid membrane behave similarly in the vicinity of the bifurcation.

In the simulations (figure 5*b*), we clearly see that for a given R, the discrepancy between the fluid and particle behaviour increases when Q_1/Q_0 decreases. On the contrary, in the quasi-two-dimensional case of the experiments, the difference between

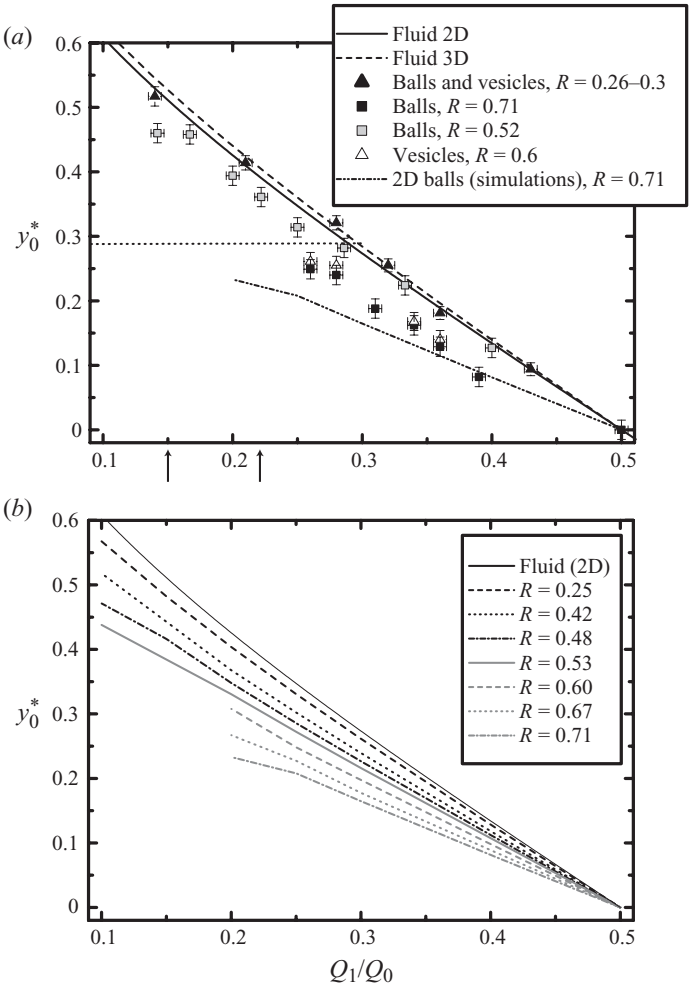

FIGURE 5. Position of the particle-separating line y_0^*. The T-bifurcation with branches of equal widths is considered. Branch 1 receives flow from high y values, so $y_0^* < y_f$ for $Q_1/Q_0 < 1/2$ indicates attraction towards the low-flow-rate branch (see also figure 1*b*). (*a*) Data from quasi-two-dimensional experiments and comparison with the two-dimensional case for one particle size. The two-dimensional and three-dimensional fluid-separating lines are shown to illustrate the low discrepancy between the two cases, as required to validate our new analysis of the literature in § 2. The horizontal dotted line shows the maximum position $y_0 = 1 - R$ for $R = 0.71$ spheres. Its intersection with the curve $y_0^*(Q_1/Q_0)$ yields the critical flow rate ratio Q_1/Q_0 below which no particle enters branch 1, the low-flow-rate branch. These expected critical flow rates for the two- and three-dimensional cases are shown by arrows. (*b*) Data from two-dimensional simulations.

the flow and the particle streamlines seems to be rather constant in a wide range of Q_1/Q_0 values. Finally, for small enough values of Q_1/Q_0, the attraction effect is more pronounced in the two-dimensional case than in the quasi-two-dimensional case, as shown in figure 5(*a*) for $R = 0.71$. This result was expected, since this effect has something to do with the non-zero size of the particle, and the real particle to channel size ratio is lower in the experiments for a given R, due to the third dimension. In all cases, below a given value of Q_1/Q_0, the critical position y_0^* would enter the depletion zone $y_0 > 1 - R$, so that no particle will eventually enter the low-flow-rate branch.

The corresponding critical Q_1/Q_0 is much lower in the two-dimensional case than in the experimental quasi-two-dimensional situation (see figure 5*a*).

4.1.2. *Discussion*

The first argument for some attraction towards one branch was initially given by Fung (see Fung 1973; Yen & Fung 1978; Fung 1993) and strengthened by recent simulations (see Yang & Zahn 2004): a sphere in the middle of the bifurcation is considered ($y_0 = 0$) and it is argued that it should go to the high-flow-rate branch since the pressure drop $P_0 - P_2$ is higher than $P_0 - P_1$ because $Q_2 > Q_1$ (see figure 1*b* for notation). This is true (we also found $y_0^* > 0$ when $Q_1 < Q_2$) but this is not the point to be discussed: if one wishes to discuss the increase in volume fraction in branch 2, therefore to compare the particles and fluid fluxes N_2 and Q_2, one needs to focus on particles in the vicinity of the fluid-separating streamline (to see whether or not they behave like the fluid) and not in the vicinity of the middle of the channel. On the other hand, this incorrectly formulated argument by Fung has led to the idea that there must be some attraction towards the high-flow-rate branch in the vicinity of the fluid-separating streamline (see Yang *et al.* 2006), which appears now in the literature as a well-established fact (see Jäggi *et al.* 2007; Kersaudy-Kerhoas *et al.* 2010).

In Barber *et al.* (2008), Fung's argument has been rejected, although it is not explained why. Arguments for attraction towards the low-flow-rate branch (that is, $P_2 > P_1$ in figure 1*b*) are given, considering particles in the vicinity of the fluid separating streamline. The authors' main idea was, first, that some pressure difference $P_0 - P_i$ builds up on each side of the particle because it travels more slowly than the fluid. Then, as the particle intercepts a relatively more important area in the low-flow-rate branch region ($y_f < y < 1$) than in the high-flow-rate region, they consider that the pressure drop is more important in the low-flow-rate region, so that $P_2 > P_1$. The authors called this effect 'daughter vessel obstruction'.

However, it is not clear in Barber *et al.* (2008) where the particles must be for this argument to be valid: they could be at the entrance of the bifurcation, in the middle of it or close to the opposite wall, since their arguments are used to explain what happens in the case of daughter branches of different widths. Indeed, we shall see that the effects can be quite different according to this position and, furthermore, the notion of 'relatively larger part intercepted' is not the key phenomenon to understand the final attraction towards the low-flow-rate branch, even though it clearly contributes to it.

To understand this, let us focus on the simulated trajectories starting around y_0^* shown in figure 6(*a*) ($R = 0.67$, $Q_1/Q_0 = 0.2$). These trajectories must be analysed in comparison with the unperturbed flow streamlines, in particular the fluid separating streamline, starting at $y = y_f$ and ending against the front wall at a stagnation point.

Particles starting around $y_0^* < y_f$ show a clear attraction towards the low-flow-rate branch (displacement along the y-axis) as they enter the bifurcation. More precisely, there are three types of motions: for low initial position y_0 (in particular $y_0 = 0$), particles travel directly into the high-flow-rate branch. Similarly, above y_0^*, the particles travel directly into the low-flow-rate branch. Between some $y_0^{**} > 0$ and y_0^*, the particles first move towards the low-flow-rate branch, but finally enter the high-flow-rate branch: the initial attraction towards the low-flow-rate branch becomes weaker and the particles eventually follow the streamlines entering the high-flow-rate branch. This non-monotonic variation of y_0 for a particle starting just below y_0^* is also seen in experiments, as shown in figure 4(*b*): the third position of the vesicle is

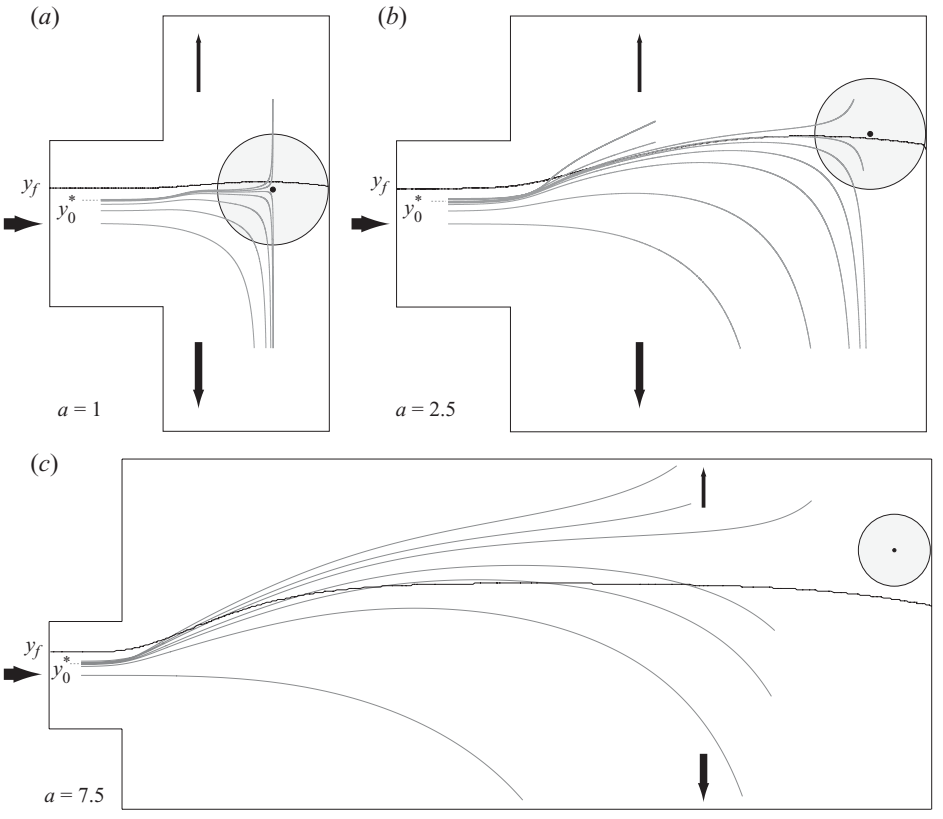

FIGURE 6. Comparison between fluid and particle trajectories in the vicinity of the bifurcation. Grey lines, some trajectories of an $R = 0.67$ particle when $Q_1/Q_0 = 0.2$ for (a) branches of equal widths, (b) daughter branches 2.5 times wider than the inlet branch and (c) daughter branches 7.5 times wider than the inlet branch. The unperturbed fluid separating streamline starting at $y = y_f$ is shown in black. The particle is shown approximately at its stagnation point.

characterized by a y_0 slightly higher than the initial one. Returning to the simulations, note that, at this level, there is still some net attraction towards the low-flow-rate branch: the particle stagnation point near the opposite wall is still below the fluid-separating streamline (that is, on the high-flow-rate side). This two-step effect is even more visible when the width $2a$ of the daughter branches is increased, so that the entrance of the bifurcation is far from the opposite wall, as shown in figure 6(b,c). The second attraction is, in such a situation, more dramatic: for $a = 7.5$, the particle stagnation point is even on the other side of the fluid-separating streamline, that is, there is some attraction towards the high-flow-rate branch. Thus, there are clearly two antagonistic effects along the trajectory. In the first case of branches of equal widths, where the opposite wall is close to the bifurcation entrance, the second attraction towards the high-flow-rate branch coexists with the attraction towards the low-flow-rate branch and finally only diminishes it.

These two effects occur in two very different situations. At the entrance of the channel, an attraction effect must be understood in terms of streamlines crossing: does a pressure difference build up orthogonally to the main flow direction? Near the opposite wall, the flow is directed towards the branches and being attracted means

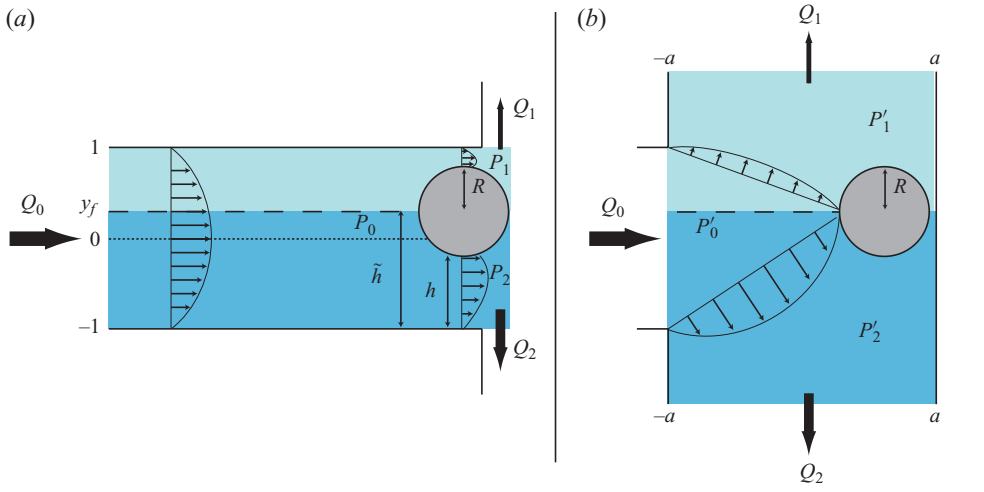

FIGURE 7. (Colour online) Schematic of the geometry considered for the two effects occurring in the bifurcation. (*a*) Entrance to the bifurcation showing attraction towards the low-flow-rate branch ($P_1 < P_2$). (*b*) Opposite wall showing attraction towards the high-flow-rate branch ($P'_1 > P'_2$).

flowing upstream or downstream. In both cases, in order to discuss whether some pressure difference builds up or not, the main feature is that, in a two-dimensional Stokes flow between two parallel walls, the pressure difference between two points along the flow direction scales like $\Delta P \propto Q/h^3$, where Q is the flow rate and h is the distance between the two walls. This scaling is sufficient to discuss in a first-order approach the two effects at stake.

The second effect is the simplest one: the sphere is placed in a quasi-elongational, but asymmetric, flow. As shown in figure 7(*b*), around the flow stagnation point, the particle movement is basically controlled by the pressure difference $P'_2 - P'_1$, which can be written $(P'_0 - P'_1) - (P'_0 - P'_2)$. Focusing on the y-component of the velocity field, which becomes all the more important as a is larger than 1, we have $P'_0 - P'_i \propto Q_i/(a-R)^3$. Around the flow stagnation point, the pressure difference $P'_2 - P'_1$ has then the same sign as $Q_1 - Q_2$ and is thus negative, which indicates attraction towards the high-flow-rate branch. For wide daughter branches, when this effect is not screened by the first one, this implies that the stagnation point for particles is above the fluid separating line, as seen in figure 6(*c*). The argument that we use here is similar to that introduced by Fung (see Fung 1993; Yang *et al.* 2006) but resolves only one part of the problem. Following these authors, it can also be pointed out that the shear stress on the sphere is non-zero: in a two-dimensional Poiseuille flow of width h, the shear rate near a wall scales as Q/h^2, so the net shear stress on the sphere is directed towards the high-flow-rate branch, making the sphere roll along the opposite wall towards this branch.

Finally, this situation is similar to that of a flow around an obstacle, which was considered by El-Kareh & Secomb (2000) as a model situation to understand what happens at the bifurcation. Indeed, the authors found that spheres are attracted towards the high-velocity side of the obstacle. However, we show here that this modelling is misleading, as it neglects the first effect, which eventually governs the net effect.

This first effect leads to an attraction towards the low-flow-rate branch. To understand this, let us consider a sphere located in the bifurcation with transverse position $y_0 = y_f$. The exact calculation of the flow around it is much too complicated, and simplifications are needed. Just as we considered the large a case to understand the second mechanism eventually leading to attraction towards the high-flow-rate branch, let us consider the small a limit to understand the first effect: as soon as the ball enters the bifurcation, it hits the front wall. On each side, we can write in a first approximation that the flow rate between the sphere and the wall scales as $Q \propto \Delta P h^3$, where $\Delta P = P_0 - P_i$ is the pressure difference between the back and the front of the sphere, and h is the distance between the sphere and the wall (see figure 7*a*).

Since the ball touches the front wall, the flow rate Q is either Q_1 or Q_2 and is, by definition of y_f, the integral of the unperturbed Poiseuille flow velocity between the wall and the $y = y_f$ line, so $Q \propto \tilde{h}^2 - \tilde{h}^3/3$, where $\tilde{h} = 1 \pm y_f$ (see figure 7*a* for notation).

We have then, on each side,

$$\Delta P \propto \frac{\tilde{h}^2 - \tilde{h}^3/3}{h^3}. \tag{4.1}$$

To make things clear, let us consider the extreme case of a flat particle: $h = \tilde{h}$. Then, $\Delta P \propto 1/\tilde{h} - 1/3$ is a decreasing function of $\tilde{h}$, that is, a decreasing function of Q. Therefore, the pressure drop is more important on the low-flow-rate side, and finally $P_1 < P_2$: there is an attraction towards the low-flow-rate branch. This is exactly the opposite result from the simple view claiming that there is some attraction towards the high-flow-rate branch since ΔP scales as Q/h^3 so as Q. Since one has to discuss what happens for a sphere in the vicinity of the separating line, Q and $\tilde{h}$ are not independent. This is the key argument. Note finally that there is no need for some obstruction arguments to build up a different pressure difference on each side. It only increases the effect since the function $\tilde{h} \mapsto (\tilde{h}^2 - \tilde{h}^3/3)/(\tilde{h} - R)^3$ decreases faster than the function $\tilde{h} \mapsto (\tilde{h}^2 - \tilde{h}^3/3)/\tilde{h}^3$. One can be even more precise and take into account the variations in the gap thickness as the fluid flows between the sphere and the wall to calculate the pressure drop by lubrication theory. Still, it is found that ΔP is a decreasing function of $\tilde{h}$.

In the more realistic case $a \simeq 1$, the flow repartition becomes more complex, and the particle velocity along the x-axis is not zero. Yet, as it reaches a low-velocity area (the velocity along the x-axis of the streamline starting at y_f drops to zero), its velocity is lower than its velocity at the same position in a straight channel. In addition, as the flow velocities between the sphere and the opposite wall are low, and since the fluid located e.g. between y_f and the top wall will eventually enter the top branch by definition, we can assume that it will mainly flow between the sphere and the top wall. Note that this is not true in a straight channel: there are no reasons for the fluid located between one wall and the $y = y_0$ line, where y_0 is the sphere lateral position, to enter completely, or to be the only fluid to enter, between the wall and the particle. Therefore, we can assume that the arguments proposed to explain the attraction towards the low-flow-rate branch remain valid, even though the net effect will be weaker.

Note, finally, that contrary to what we discussed for the second effect, the particle rotation probably plays a minor role here, as in this geometry the shear stress exerted by the fluid on the particle will mainly result in a force acting parallel to the x-axis.

Finally, this separation into two effects can be used to discuss a scenario for bifurcations with channels of different widths: if the inlet channel is broadened, the first effect becomes less strong while the second one is not modified, which results in a weaker attraction towards the low-flow-rate branch. If the outlet channels are broadened, as in figure 6(b,c), it becomes more subtle. Let us start again with the second effect (migration upstream or downstream) before the first effect (transverse migration). As seen in figure 6, the position of the particle stagnation point (relative to the flow-separating line) is an increasing function of a, so the second effect is favoured by the broadening of the outlets: for $a \to \infty$, we end up with the problem of flow around an obstacle, while for small a, one cannot write that the width of the gap between the ball and the wall is just $a - R$, therefore independent from Q_i, as it also depends on the y-position of the particle relative to y_0'. In other words, in such a situation, the second effect is screened by the first effect. On the other hand, as a increases, the distance available for transverse migration becomes larger, which could favour the first effect, although the slowdown of the particle at the entrance of the bifurcation becomes less pronounced.

Finally, it appears difficult to predict the consequences of an outlet broadening: for instance, in our two-dimensional simulations presented in figure 6 ($R = 0.67$, $Q_1/Q_0 = 0.2$), y_0^* varies from 0.27 when the outlet half-width a is equal to 1, to 0.31 when a is equal to 2.5 and drops down to 0.22 for $a = 7.5$. Note that the net effect is always an attraction towards the low-flow-rate branch ($y_0^* < y_f$).

For daughter branches of different widths, it was illustrated in Barber *et al.* (2008) that the narrower branch is favoured. This can be explained through the second effect (see figure 7b): the pressure drop $P_0' - P_i' \propto Q_i/(a - R)^3$ increases when the channel width decreases, which favours the narrower branch even in the case of equal flow rates between the branches.

4.2. *The consequences for the final distribution*

As there is some attraction towards the low-flow-rate branch, we could expect some enrichment of the low-flow-rate branch. However, as already discussed, even in the most uniform situation, the presence of a free layer near the walls will favour the high-flow-rate branch. We discuss now, through our simulations, the final distribution that results from these two antagonistic effects.

As in most previous papers in the literature, we focus on the case of uniform number density of particles in the inlet ($n(y) = 1$ in (1.1)). In order to compute the final splitting N_1/N_0 of the incoming particles as a function of flow rate ratio Q_1/Q_0, one needs to know, according to (1.1), the position y_0^* of the particle-separating line and the velocity u_x^* of the particles in the inlet channel. From figure 5, we see that y_0^* depends roughly linearly on (Q_1/Q_0–1/2), so we will consider a linear fit of the calculated data in order to get values for all Q_1/Q_0. The longitudinal velocity u_x^* was computed for all studied particles as a function of transverse position y_0. As shown in figure 8, the function $u_x^*(y_0)$ is well described by a quartic function $u_x^*(y_0) = \alpha y_0^4 + \beta y_0^2 + \gamma$, which is an approximation also used in Barber *et al.* (2008). Values for the fitting parameters for this velocity profile and for the linear relationship $y_0^* = \xi \times (Q_1/Q_0 - 1/2)$ are given in table 1.

The evolution of N_1/N_0 as a function of Q_1/Q_0 for two-dimensional rigid spheres is shown in figure 9 for two representative radii. By symmetry, considering $Q_1 < Q_2$ is sufficient. In order to discuss the enrichment of particles in the high-flow-rate branch (branch 2 then), it is also convenient to consider directly the volume fraction variation $\Phi_2/\Phi_0 = (N_2/Q_2)/(N_0/Q_0)$.

R	0	0.25	0.42	0.48	0.53	0.60	0.67	0.71	0.80
α	0	−0.96	−3.45	−4.77	−6.33	−9.52	−11.6	−12.6	–
β	−1	−0.85	−0.65	−0.70	−0.64	−0.61	−0.71	−0.73	–
γ	1	0.96	0.91	0.89	0.87	0.84	0.81	0.79	0.75
ξ	–	−1.35	−1.25	−1.17	−1.09	−1.01	−0.90	−0.81	–

TABLE 1. Values for the fitting parameters (α, β, γ) for the longitudinal velocity $u_x^*(y_0) = \alpha y_0^4 + \beta y_0^2 + \gamma$ of a two-dimensional sphere of radius R in a Poiseuille flow of imposed velocity at infinity $u_x(y) = 1 - y^2$; for $R = 0.80$, the velocity profile is too flat to be reasonably fitted by a three-parameter law, since all velocities are equal to 0.75 ± 0.005 in the explored interval $y_0 \in [-0.15; 0.15]$. We also give the values for the fitting parameter ξ of the linear relationship between the particle separating line position y_0^* and flow rate ratios: $y_0^* = \xi \times (Q_1/Q_0 - 1/2)$. For $R = 0.8$, the strong confinement leads to numerical problems as the sphere approaches the walls.

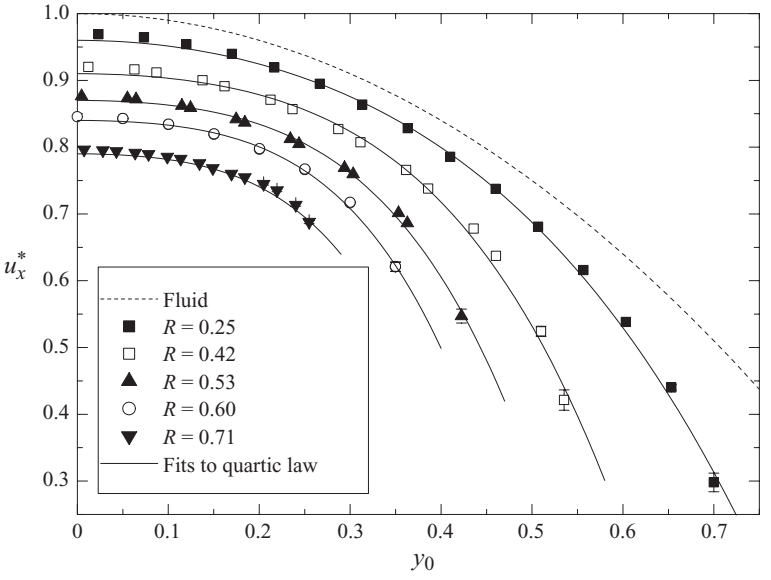

FIGURE 8. Some longitudinal velocity profiles $u_x^*(y_0)$ for two-dimensional spheres of different radii R in the inlet channel, where a Poiseuille flow of velocity $u_x(y) = 1 - y^2$ is imposed at infinity. The full lines show the fits by the quartic law $u_x^*(y_0) = \alpha y_0^4 + \beta y_0^2 + \gamma$.

When $Q_1/Q_0 = 1/2$, the particle flow splits equally into the two branches: $N_1 = N_0$ and $\Phi_2 = \Phi_0$. For all explored sizes of spheres, when the flow rate in branch 1 decreases, there is an enrichment of particles in branch 2, which is precisely the Zweifach–Fung effect: $N_1/N_0 < Q_1/Q_0$ or $\Phi_2/\Phi_0 > 1$. Then, even in the most homogeneous case, the attraction towards the low-flow-rate branch is not strong enough to counterbalance the depletion effect that favours the high-flow-rate branch. However, this attraction effect cannot be considered as negligible, in particular for large particles: while, when the particles follow their underlying fluid streamline, the maximum enrichment in the high-flow-rate branch would be around 40 % for $R = 0.71$, it drops down to less than 17 % in reality. Similarly, the critical flow rate ratio Q_1/Q_0 below which no particle enters into branch 1 is greatly shifted: from around 0.29 to around 0.15 for $R = 0.71$. For smaller spheres ($R = 0.42$), this asymmetry in the distribution between the two

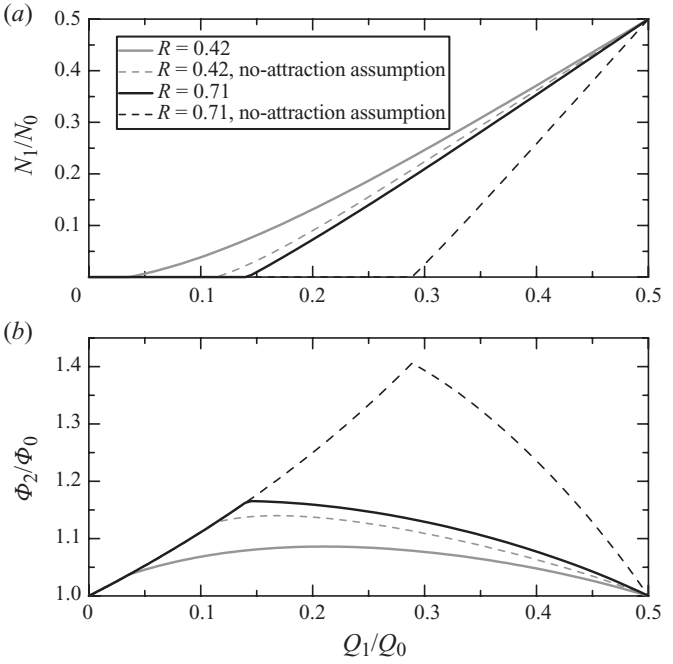

FIGURE 9. Final particle distributions. Full lines, spheres' relative distribution N_1/N_0 (a) and volume fraction Φ_2/Φ_0 (b) as a function of the flow rate distribution Q_1/Q_0 from our two-dimensional simulations for two representative radii $R = 0.42$ and $R = 0.71$. The curves are straightforwardly derived from (1.1) and (1.2) and computed values of y_0^* and u_x^* (table 1). The results are compared with the hypothesis where the particles would follow the streamlines ($y_0^* = y_f$) (dashed lines).

branches is weak: while the maximum enrichment in the high-flow-rate branch would be around 15 % in a no-attraction case, it drops to less than 8 % due to the attraction towards the low-flow-rate branch.

When the flow Q_1 is equal to zero or $Q_0/2$, Φ_2 is equal to Φ_0; thus, there is a maximal enrichment for some flow rate ratio between 0 and 1/2. Starting from $Q_1/Q_0 = 0.5$, the increase in Φ_2 with the decrease of Q_1 is mainly due to the decrease of the relative importance of the free layer near the wall on the side of branch 2. Two mechanisms are then responsible for the decrease of Φ_2 when Q_1 goes on decreasing: first, when no particle can enter the low-flow-rate branch because its hypothetical separation line y_0^* is above its maximum position $1 - R$, then the high-flow-rate branch receives only additional solvent when Q_1/Q_0 decreases and its particles are more diluted. Then, all curves fall onto the same curve $\Phi_2/\Phi_0 = 1/(1 - Q_1/Q_0)$ corresponding to $N_1 = 0$ (or $N_2 = N_0$), which results in a sharp variation as Q_1/Q_0 goes through the critical flow rate ratio. A smoother mechanism is also to be taken into account here, which is the one that finally determines the maximum for smaller R. As Q_1/Q_0 decreases, branch 2 recruits fluid and particles that are closer and closer to the opposite wall. As seen in figure 8, the discrepancy between the flow and particle velocities increases near the walls, so that N_2 increases less than Q_2: the resulting concentration in branch 2 finally decreases.

Finally, for applicative purposes, the consequences of the attraction towards the low-flow-rate branch are twofold: if one wishes to obtain a particle-free fluid (e.g. plasma without red blood cells), one has to set Q_1 low enough so that $N_1 = 0$. Because

of attraction towards the low-flow-rate branch, this critical flow rate is decreased and the efficiency of the process is lowered. If one prefers to concentrate particles, then one must find the maximum of the Φ_2/Φ_0 curve. This maximum is lowered and shifted by the attraction towards the low-flow-rate branch (see figure 9). Note that for small spheres (e.g. $R=0.42$), the position of the maximum does not correspond to the point at which N_1 vanishes; in addition, the shift direction of the maximum position depends on the sphere size: while it shifts to lower Q_1/Q_0 values for $R=0.71$, it shifts to higher values for $R=0.42$.

The choice of the geometry, within our symmetric frame, can also greatly modify the efficiency of a device. Since the depletion effect eventually governs the final distribution, narrowing the inlet channel is the first requirement. On the other hand, it also increases the attraction towards the low-flow-rate branch, but one can try to diminish it. As discussed in the preceding section, this can be done by widening reasonably the daughter branches. For instance, if their half-width is not 1 but 2.5, as in figure 6(*b*), the slope ξ in the law $y_0^*=\xi\times(Q_1/Q_0-1/2)$ increases by around 15 % for $R=0.67$. The critical Q_1/Q_0 below which no particle enters the low-flow-rate branch increases from 0.13 to 0.19, which is good for fluid–particle separation, and the maximum enrichment Φ_2/Φ_0 that can be reached is 22 % instead of 15 %. Alternatively, since the attraction is higher in two dimensions than in three, we can also infer that considering thicker channels, which does not modify the depletion effect, can greatly improve the final result. Note that this conclusion would have been completely different in the case of the high-flow-rate branch enrichment due to some attraction towards it, as claimed in some papers: in such a case, confining as much as possible would have been required, as it increases all kinds of cross-streamline drifts.

4.3. *Consistency with the literature*

We now come back to the previous studies already discussed in § 2 in order to check the consistency between them and our results.

The only paper that dealt with the position of the particle-separating streamline was by Barber *et al.* (2008), where a symmetric Y-shaped bifurcation was studied (branches leaving the bifurcation with a 45° angle relative to the inlet channel, see figure 1*a*). In figure 10(*a*), we compare their results with our simulations in a similar geometry. The agreement between the two simulations (based on two different methods) is very good, except for large particles ($R=0.67$) and low Q_1/Q_0. Note that Barber *et al.* (2008) have chosen to consider branches whose widths follow the law $w_0^3=w_1^3+w_2^3$, where w_0 is the width of the inlet branch and w_1 and w_2 are the widths of the daughter branches. This law has been shown to describe approximately the relationship between vessel diameters in the arteriolar network (see Mayrovitz & Roy 1983). With our notation, they thus consider $a=\sqrt[3]{1/2}\simeq 0.79$, while we focused on $a=1$ in order to compare with the T-shaped bifurcation. In addition, their apex has a radius 0.75 (for the $R=0.67$ case) while ours is sharper (with radius of 0.1). These differences seem to impact only partly on the results, as discussed above. We can expect this slight discrepancy to be due to the treatment of the numerical singularities that appear when the particle is close to one wall. For $R=0.67$, the maximum position y_0 is 0.33, which is close to the separating streamline position.

It is also interesting to compare our results in the Y-shaped bifurcation with the results in the T geometry, which was chosen to make the discussion easier. We can see that, for low enough Q_1/Q_0, the attraction towards the low-flow-rate branch is slightly higher. This can be understood by considering a particle with initial position y_0 slightly below the critical position y_0^* found in the T geometry: in the latter

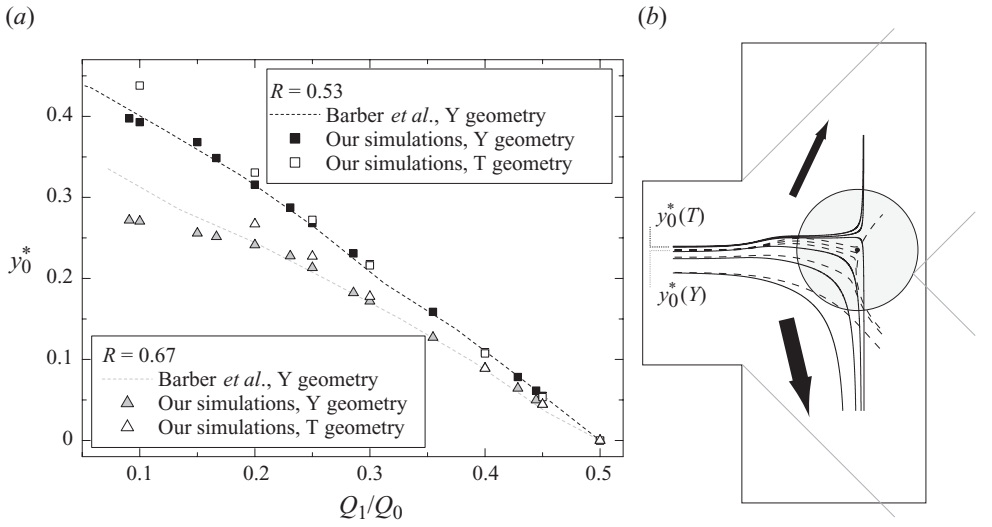

FIGURE 10. (*a*) Position of the particle separation line y_0^* in a symmetric Y-shaped bifurcation: according to Barber *et al.* (2008) (data extracted from their figure 4) and according to our simulations. The results for similar spheres in our T geometry are also shown. (*b*) Trajectories from our simulations in the T- and Y-shaped bifurcations, for similar sphere size ($R = 0.67$) and flow rate ratio ($Q_1/Q_0 = 0.2$). Full lines, T geometry; dashed lines, Y geometry. The corresponding separating streamline positions (respectively $y_0^*(T)$ and $y_0^*(Y)$) are also indicated. The sphere shown is located at its stagnation point y_0' (see figure 6) in the Y geometry.

geometry, it will eventually enter the high-flow-rate branch, by definition of y_0^*. As shown in figure 10(*b*), in the Y geometry, this movement is hindered by the apex since the final attraction towards the high-flow-rate branch occurs near the opposite wall (the second effect discussed in § 4.1.2). Finally, from this comparison we see that comparing results in T and symmetric Y geometry is relevant but for highly asymmetric flow distributions.

In § 2, the analysis of the two-dimensional simulations for $R = 0.5$ spheres in Audet & Olbricht (1987) showed that there should be some attraction towards the low-flow-rate branch. Our simulations for $R = 0.48$ showed that this effect is non-negligible (figure 5*b*) and modifies significantly the final distribution (figure 9). Finally, we can see in figure 11 that our simulations give results similar to those of Audet & Olbricht (1987).

As for the experiments presented in Yang *et al.* (2006) for $R = 0.46$, we showed that the final distribution was consistent with a no-attraction assumption. As we showed in figure 5(*a*), in a three-dimensional case, the attraction towards the low-flow-rate region is weak for spheres of radius $R \simeq 0.5$ or smaller, which is again consistent with the results of Yang *et al.* (2006). Note that, while their results were considered by the authors as a basis to discuss some attraction effect towards the high-flow-rate branch, we see that their final distributions are just reminiscent of the depletion effect in the inlet channel.

The other consistent set of studies in the literature deals with large balls in three-dimensional channels. We have studied balls of radius $R = 0.71$ that stop entering branch 1 when $Q_1/Q_0 \lesssim 0.22$ (figure 5*a*), while this critical flow rate would be around 0.29 if they followed the fluid streamlines. This critical flow rate is expected to be slightly higher for larger balls of radius $R \simeq 0.8$, but far lower than 0.35, which

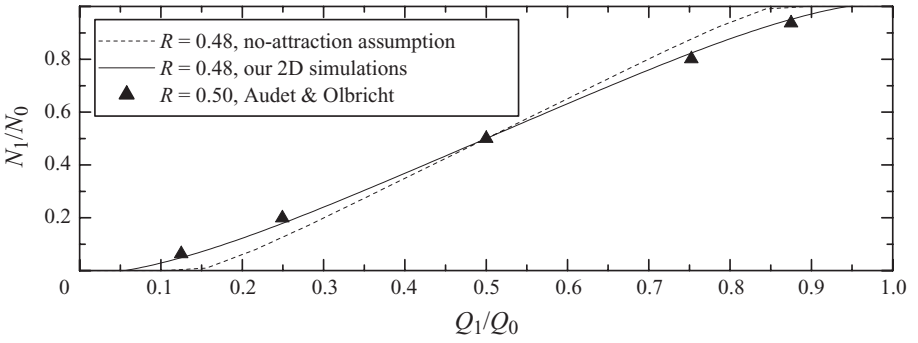

FIGURE 11. Particle distribution as a function of flow rate ratios for spheres of medium size, according to simulations of this paper and Audet & Olbricht (1987) (same data as plotted in figure 2).

would be the no-attraction case. In the experiments of Roberts & Olbricht (2006), some balls are still observed in branch 1 when $Q_1/Q_0 \simeq 0.22$ (figure 2), indicating a stronger attraction effect towards the low-flow-rate branch, which can be associated with the fact that the authors considered a square cross-sectional channel, while the confinement in the third direction is $0.5 < 0.71$ in our case. The experiments with circular cross-sectional channels lead to contradictory results: in Chien *et al.* (1985) and Ditchfield & Olbricht (1996), the results were consistent with a no-attraction assumption; therefore, they are in contradiction with our results. On the contrary, in Roberts & Olbricht (2003), the critical flow rate for $R = 0.77$ is around 0.2, which would show a stronger attraction than in our case. Note that all these apparently contradictory observations are to be considered keeping in mind that the data of N_1/N_0 as a function of Q_1/Q_0 are sometimes very noisy in the papers cited.

5. Conclusion

In this paper, we have focused explicitly on the existence and direction of some cross-streamline drift of particles in the vicinity of a bifurcation with different flow rates in the daughter branches. A new analysis of some previous unexploited results from the literature first gave us some indications on the possibility of an attraction towards the low-flow-rate branch.

Then, the first direct experimental proof of attraction towards the low-flow-rate branch was shown and arguments for this attraction were given with the help of two-dimensional simulations. In particular, we showed that this attraction is the result of two antagonistic effects: the first effect, which takes place at the entrance of the bifurcation, induces migration towards the low-flow-rate branch, while the second effect takes place near the stagnation point and induces migration towards the high-flow-rate branch but is not strong enough, in standard configurations of branches of comparable sizes, to counterbalance the first effect.

Only the second effect was previously considered in most papers in the literature, which has led to the misleading idea that the enrichment of particles in the high-flow-rate branch is due to some attraction towards it. On the contrary, it had been argued by Barber *et al.* (2008) that there should be some attraction towards the low-flow-rate branch. By distinguishing the two effects mentioned above, we have tried to clarify their statements.

In the second step, we have discussed the consequences of such an attraction on the final distribution of particles. It appears that the attraction is not strong enough, even in a two-dimensional system where it is stronger, to counterbalance the impact of the depletion effect. Even in the most homogeneous case where the particles are equally distributed across the channel but cannot approach the wall closer than their radius, the existence of a free layer near the walls favours the high-flow-rate branch, which eventually receives more particles than fluid.

However, these two antagonistic phenomena are of comparable importance, and neither can be neglected: the increase in the particle volume fraction in the high-flow-rate branch is typically divided by two because of the attraction effect. On the other hand, the initial distribution is a key parameter for the prediction of the final splitting. For deformable particles, initial lateral migration can induce a narrowing of their distribution, which will eventually favour the high-flow-rate branch. For instance, Barber *et al.* (2008) had to adjust the free layer width in their simulations in order to fit experimental data on blood flow. On the other hand, in a network of bifurcations, the initially centred particles will find themselves close to one wall after the first bifurcation, which can favour a low-flow-rate branch in a second bifurcation.

Note, finally, that as seen in Enden & Popel (1992), these effects become weaker when the confinement decreases. Typically, as soon as the sphere diameter is less than half the channel width, the variations of volume fraction do not exceed a few per cent.

For applicative purposes, the consequences of this attraction have been discussed and some prescriptions have been proposed. Of course, one can go further than our symmetric case and modify the angle between the branches, or consider many-branch bifurcations, and so on. However, the T-bifurcation case allowed us to distinguish between two goals: concentrating a population of particles or obtaining a particle-free fluid. The optimal configuration can be different according to the chosen goal. Similar considerations are also valid regarding sorting in polydisperse suspensions, which is an important activity (see Pamme 2007): getting an optimally concentrated suspension of large particles might not be compatible with getting a suspension of small particles free of large particles.

Now that the case of spherical particles in a symmetric bifurcation has been studied and the framework well established, we believe that quantitative discussions could be made in the future about the other parameters that we put aside here. In particular, discussing the effect of the deformability of the particles is a challenging task if one only considers the final distribution data, as the deformability modifies the initial distribution, but most probably also the attraction effect. In a network, the importance of these contributions will be different according, in particular, to the distance between two bifurcations, so they must be discussed separately.

Considering concentrated suspensions is of course the next challenging issue. Particles close to each other will obviously hydrodynamically interact, but so will distant particles, through the modification of the effective resistance to flow of the branches. In such a situation, considering pressure-driven or flow-rate-driven fluids will be different.

For concentrated suspensions of deformable particles in a network, like blood in the circulatory system, the relevance of a particle-based approach can be questioned. Historical models for the major blood flow phenomena are continuum models with some *ad hoc* parameters, which must be somehow related to the intrinsic mechanical properties of the blood cells (for a recent example, see Obrist *et al.* 2010). Building up a bottom-up approach in such a system is a long quest. For dilute suspensions,

some links between the microscopic dynamics of lipid vesicles and the rheology of a suspension have been recently established (see Danker & Misbah 2007; Vitkova *et al.* 2008; Ghigliotti, Biben & Misbah 2010). For red blood cells, which exhibit qualitatively similar dynamics (see Abkarian *et al.* 2007; Deschamps *et al.* 2009; Dupire, Abkarian & Viallat 2010; Farutin, Biben & Misbah 2010; Noguchi 2010), we can hope that such a link will soon be established, following Vitkova *et al.* (2008). For confined and concentrated suspensions, the distribution is known to be non-homogeneous, which has direct consequences on the rheology (the Fahraeus–Lindquist effect). Once again, while empirical macroscopic models are able to describe this reality, establishing the link between the viscosity of the suspension and the local dynamics is still a challenging issue. The final distribution of the flowing bodies is the product of a balance between migration towards the centre, as discussed in the Introduction, and interactions between them that can broaden the distribution (see Kantsler, Segre & Steinberg 2008; Podgorski *et al.* 2010). The presence of deformable boundaries also needs to be taken into account, as shown in Beaucourt *et al.* (2004). In the meantime, the development of simulation techniques for quantitative three-dimensional approaches is a crucial task, which is becoming more and more feasible (see McWhirter, Noguchi & Gompper 2009; Biben, Farutin & Misbah 2011).

The authors thank G. Ghigliotti for his final reading and acknowledge financial support from ANR MOSICOB and CNES.

Appendix. Derivation of the variational formulation

In this appendix, details of the derivation of (3.13)–(3.15) from (3.10)–(3.12) are given.

First, we introduce the scalar product in $L^2(\Omega_f)^2$ as follows:

$$\forall \boldsymbol{f}, \boldsymbol{g} \in L^2(\Omega_f)^2, \quad \langle \boldsymbol{f}, \boldsymbol{g} \rangle_{L^2(\Omega_f)^2} = \int_{\Omega_f} \boldsymbol{f} \cdot \boldsymbol{g}. \tag{A 1}$$

The variational formulation of the problem (3.10)–(3.12) is obtained by taking the scalar product of (3.10) in $L^2(\Omega_f)^2$ with a test function $\boldsymbol{v} \in H_0^1(\Omega_f)^2$ and we multiply (3.11) by a test function $q \in L_0^2(\Omega)$. It leads to the following problem: find $(\boldsymbol{u}, p) \in H^1(\Omega_f)^2 \times L_0^2(\Omega_f)$ such that

$$-2\nu \int_{\Omega_f} (\nabla \cdot \boldsymbol{\tau}(\boldsymbol{u})) \cdot \boldsymbol{v} + \int_{\Omega_f} \nabla p \cdot \boldsymbol{v} = 0, \quad \forall \boldsymbol{v} \in H_0^1(\Omega_f)^2, \tag{A 2}$$

$$\int_{\Omega_f} q \nabla \cdot \boldsymbol{u} = 0, \quad \forall q \in L_0^2(\Omega_f), \tag{A 3}$$

$$\boldsymbol{u} = \boldsymbol{f} \quad \text{on } \partial\Omega_f. \tag{A 4}$$

Applying Green's formula to (A 2), we obtain

$$2\nu \int_{\Omega_f} \boldsymbol{\tau}(\boldsymbol{u}) : \nabla \boldsymbol{v} - 2\nu \int_{\partial\Omega_f} \boldsymbol{\tau}(\boldsymbol{u}) \boldsymbol{n} \cdot \boldsymbol{v} - \int_{\Omega_f} p \nabla \cdot \boldsymbol{v} + \int_{\partial\Omega_f} p \boldsymbol{v} \cdot \boldsymbol{n} = 0, \tag{A 5}$$

where $\boldsymbol{n}$ denotes the outer unit normal on $\partial\Omega_f$. Taking into account the fact that $\boldsymbol{v}$ vanishes on $\partial\Omega_f$ (recall that we have chosen the test function $\boldsymbol{v} \in H_0^1(\Omega_f)^2$), the

problem (A 2)–(A 4) is now equivalent to this one: find $(\boldsymbol{u}, p) \in H^1(\Omega_f)^2 \times L^2_0(\Omega_f)$ such that

$$2\nu \int_{\Omega_f} \boldsymbol{\tau}(\boldsymbol{u}) : \nabla \boldsymbol{v} - \int_{\Omega_f} p \nabla \cdot \boldsymbol{v} = 0, \quad \forall \boldsymbol{v} \in H^1_0(\Omega_f)^2, \tag{A 6}$$

$$\int_{\Omega_f} q \nabla \cdot \boldsymbol{u} = 0, \quad \forall q \in L^2_0(\Omega_f), \tag{A 7}$$

$$\boldsymbol{u} = \boldsymbol{f} \quad \text{on } \partial\Omega_f. \tag{A 8}$$

Note that $\boldsymbol{\tau}(\boldsymbol{u})$ is symmetric ($\boldsymbol{\tau}(\boldsymbol{u}) : \nabla \boldsymbol{v} = \boldsymbol{\tau}(\boldsymbol{u}) : (\nabla \boldsymbol{v})^t$). So we can write $\boldsymbol{\tau}(\boldsymbol{u}) : \nabla \boldsymbol{v} = \boldsymbol{\tau}(\boldsymbol{u}) : \boldsymbol{\tau}(\boldsymbol{v})$. Finally, the variational formulation of our initial problem (3.1)–(3.3) is given by: find $(\boldsymbol{u}, p) \in H^1(\Omega_f)^2 \times L^2_0(\Omega_f)$ such that

$$2\nu \int_{\Omega_f} \boldsymbol{\tau}(\boldsymbol{u}) : \boldsymbol{\tau}(\boldsymbol{v}) - \int_{\Omega_f} p \nabla \cdot \boldsymbol{v} = 0, \quad \forall \boldsymbol{v} \in H^1_0(\Omega_f)^2, \tag{A 9}$$

$$\int_{\Omega_f} q \nabla \cdot \boldsymbol{u} = 0, \quad \forall q \in L^2_0(\Omega_f), \tag{A 10}$$

$$\boldsymbol{u} = \boldsymbol{f} \quad \text{on } \partial\Omega_f. \tag{A 11}$$

Remark 2. *As we have*

$$\boldsymbol{\tau}(\boldsymbol{u}) : \boldsymbol{\tau}(\boldsymbol{v}) = \boldsymbol{\tau}(\boldsymbol{u}) : \nabla \boldsymbol{v} = \tfrac{1}{2} \nabla \boldsymbol{u} : \nabla \boldsymbol{v} + \tfrac{1}{2} (\nabla \boldsymbol{u})^t : \nabla \boldsymbol{v}, \tag{A 12}$$

the first integral in (A 9) can be rewritten thanks to this identity

$$\int_{\Omega_f} \boldsymbol{\tau}(\boldsymbol{u}) : \boldsymbol{\tau}(\boldsymbol{v}) = \frac{1}{2} \int_{\Omega_f} \nabla \boldsymbol{u} : \nabla \boldsymbol{v}. \tag{A 13}$$

Indeed, by integration by parts and using the incompressibility constraint $\nabla \cdot \boldsymbol{u} = 0$, *we have* $\int_{\Omega_f} (\nabla \boldsymbol{u})^t : \nabla \boldsymbol{v} = 0$. *Thus, we can retrieve the formulation of our problem as a minimization of a kind of energy. The velocity field* $\boldsymbol{u}$ *is then the solution of this problem*

$$\boldsymbol{J}(\boldsymbol{u}) = \inf_{\substack{\boldsymbol{v} \in H^1(\Omega_f)^2 \\ \nabla \cdot \boldsymbol{v} = 0, \boldsymbol{v}_{|\partial\Omega_f} = \boldsymbol{f}}} \boldsymbol{J}(\boldsymbol{v}), \tag{A 14}$$

where

$$\boldsymbol{J}(\boldsymbol{v}) = \frac{1}{2} \nu \int_{\Omega_f} \nabla \boldsymbol{v} : \nabla \boldsymbol{v} = \nu \int_{\Omega_f} \boldsymbol{\tau}(\boldsymbol{v}) : \boldsymbol{\tau}(\boldsymbol{v}). \tag{A 15}$$

REFERENCES

Abkarian, M., Faivre, M. & Viallat, A. 2007 Swinging of red blood cells under shear flow. *Phys. Rev. Lett.* **98**, 188302.

Abkarian, M., Lartigue, C. & Viallat, A. 2002 Tank treading and unbinding of deformable vesicles in shear flow: determination of the lift force. *Phys. Rev. Lett.* **88**, 068103.

Angelova, M. I., Soleau, S., Meleard, P., Faucon, J. F. & Bothorel, P. 1992 Preparation of giant vesicles by external AC electric fields: kinetics and applications. *Prog. Colloid. Polym. Sci.* **89**, 127–131.

Asmolov, E. S. 2002 The inertial lift on a small particle in a weak-shear parabolic flow. *Phys. Fluids* **14**, 15–28.

Audet, D. M. & Olbricht, W. L. 1987 The motion of model cells at capillary bifurcations. *Microvasc. Res.* **33**, 377–396.

Bagchi, P. 2007 Mesoscale simulation of blood flow in small vessels. *Biophys. J.* **92**, 1858–1877.

Balvin, M., Sohn, E., Iracki, T., Drazer, G. & Frechette, J. 2009 Directional locking and the role of irreversible interactions in deterministic hydrodynamics separations in microfluidic devices. *Phys. Rev. Lett.* **103**, 078301.

Barber, J. O., Alberding, J. P., Restrepo, J. M. & Secomb, T. W. 2008 Simulated two-dimensional red blood cell motion, deformation, and partitioning in microvessel bifurcations. *Ann. Biomech. Engng* **36**, 1690–1698.

Beaucourt, J., Rioual, F., Séon, T., Biben, T. & Misbah, C. 2004 Steady to unsteady dynamics of a vesicle in a flow. *Phys. Rev.* E **69**, 011906.

Biben, T., Farutin, A. & Misbah, C. 2011 Numerical study of 3D vesicles under flow: discovery of new peculiar behaviors. *Phys. Rev.* E (in press) arXiv:0912.4702.

Bugliarello, G. & Hsiao, G. C. C. 1964 Phase separation in suspensions flowing through bifurcations: a simplified hemodynamic model. *Science* **143**, 469–471.

Callens, N., Minetti, C., Coupier, G., Mader, M.-A., Dubois, F., Misbah, C. & Podgorski, T. 2008 Hydrodynamic lift of vesicles under shear flow in microgravity. *Europhys. Lett.* **83**, 24002.

Carr, R. T. & Wickham, L. L. 1990 Plasma skimming in serial microvascular bifurcations. *Microvasc. Res.* **40**, 179–190.

Chesnutt, J. K. W. & Marshall, J. S. 2009 Effect of particle collisions and aggregation on red blood cell passage through a bifurcation. *Microvasc. Res.* **78**, 301–313.

Chien, S., Tvetenstrand, C. D., Epstein, M. A. & Schmid-Schonbein, G. W. 1985 Model studies on distributions of blood cells at microvascular bifurcations. *Am. J. Physiol. Heart Circ. Physiol.* **248**, H568–H576.

Coupier, G., Kaoui, B., Podgorski, T. & Misbah, C. 2008 Noninertial lateral migration of vesicles in bounded Poiseuille flow. *Phys. Fluids* **20**, 111702.

Danker, G. & Misbah, C. 2007 Rheology of a dilute suspension of vesicles. *Phys. Rev. Lett.* **98**, 088104.

Danker, G., Vlahovska, P. M. & Misbah, C. 2009 Vesicles in Poiseuille flow. *Phys. Rev. Lett.* **102**, 148102.

Davis, J. A., Inglis, D. W., Morton, K. J., Lawrence, D. A., Huang, L. R., Chou, S. Y., Sturm, J. C. & Austin, R. H. 2006 Deterministic hydrodynamics: taking blood apart. *Proc. Natl Acad. Sci. USA* **103**, 14779–14784.

Dellimore, J. W., Dunlop, M. J. & Canham, P. B. 1983 Ratio of cells and plasma in blood flowing past branches in small plastic channels. *Am. J. Physiol. Heart Circ. Physiol.* **244**, H635–H643.

Deschamps, J., Kantsler, V., Segre, E. & Steinberg, V. 2009 Dynamics of a vesicle in general flow. *Proc. Natl Acad. Sci. USA* **106**, 11444.

Ditchfield, R. & Olbricht, W. L. 1996 Effects of particle concentration on the partitioning of suspensions at small divergent bifurcations. *J. Biomech. Engng* **118**, 287–294.

Dupire, J., Abkarian, M. & Viallat, A. 2010 Chaotic dynamics of red blood cells in a sinusoidal flow. *Phys. Rev. Lett.* **104**, 168101.

El-Kareh, A. W. & Secomb, T. W. 2000 A model for red blood cell motion in bifurcating microvessels. *Intl J. Multiphase Flow* **26**, 1545–1564.

Eloot, S., De Bisschop, F. & Verdonck, P. 2004 Experimental evaluation of the migration of spherical particles in three-dimensional Poiseuille flow. *Phys. Fluids* **16**, 2282–2293.

Enden, G. & Popel, A. S. 1992 A numerical study of the shape of the surface separating flow into branches in microvascular bifurcations. *J. Biomech. Engng* **114**, 398–405.

Engl, W., Roche, M., Colin, A., Panizza, P. & Ajdari, A. 2005 Droplet traffic at a simple junction at low capillary numbers. *Phys. Rev. Lett.* **95**, 208304.

Fan, R., Vermesh, O., Srivastava, A., Yen, B., Qin, L., Ahmad, H., Kwong, G. A., Liu, C.-C., Gould, J., Hood, L. & Heath, J. R. 2008 Integrated barcode chips for rapid, multiplexed analysis of proteins in microliter quantities of blood. *Nature Biotech.* **26**, 1373–1378.

Farutin, A., Biben, T. & Misbah, C. 2010 Analytical progress in the theory of vesicles under linear flow. *Phys. Rev.* E **81**, 061904.

Fenton, B. M., Carr, R. T. & Cokelet, G. R. 1985 Nonuniform red cell distribution in 20 to 100 μm bifurcations. *Microvasc. Res.* **29**, 103–126.

Frechette, J. & Drazer, G. 2009 Directional locking and deterministic separation in periodic arrays. *J. Fluid Mech.* **627**, 379–401.

Fung, Y. C. 1973 Stochastic flow in capillary blood vessels. *Microvasc. Res.* **5**, 34–48.

Fung, Y. C. 1993 *Biomechanics: Mechanical Properties of Living Tissues*. Springer.

Ghigliotti, G., Biben, T. & Misbah, C. 2010 Rheology of a dilute two-dimensional suspension of vesicles. *J. Fluid Mech.* **653**, 489–518.

Girault, V. & Raviart, P.A. 1986 *Finite Element Methods for Navier–Stokes Equations: Theory and Algorithms*. Springer.

Griggs, A. J., Zinchenko, A. Z. & Davis, R. H. 2007 Low-Reynolds-number motion of a deformable drop between two parallel plane walls. *Intl J. Multiphase Flow* **33**, 182–206.

Guibert, R., Fonta, C. & Plouraboue, F. 2010 A new approach to model confined suspensions flows in complex networks: application to blood flow. *Trans. Porous Med.* **83**, 171–194.

Hecht, F. & Pironneau, O. 2010 A finite element software for PDEs: freeFEM++. Available at: http://www.freefem.org/.

Inglis, D. W. 2009 Efficient microfluidic particle separation arrays. *Appl. Phys. Lett.* **94**, 013510.

Jäggi, R. D., Sandoz, R. & Effenhauser, C. S. 2007 Microfluidic depletion of red blood cells from whole blood in high-aspect-ratio microchannels. *Microfluid Nanofluid* **3**, 47–53.

Janela, J., Lefebvre, A. & Maury, B. 2005 A penalty method for the simulation of fluid-rigid body interaction. In *ESAIM: Proc* (ed. E. Cancès & J.-F. Gerbeau), vol. 14, pp. 115–123. ESAIM.

Jousse, F., Farr, R., Link, D. R., Fuerstman, M. J. & Garstecki, P. 2006 Bifurcation of droplet flows within capillaries. *Phys. Rev.* E **74**, 036311.

Kantsler, V., Segre, E. & Steinberg, V. 2008 Dynamics of interacting vesicles and rheology of vesicle suspension in shear flow. *Europhys. Lett.* **82**, 58005.

Kaoui, B., Coupier, G., Misbah, C. & Podgorski, T. 2009 Lateral migration of vesicles in microchannels: effects of walls and shear gradient. *Houille Blanche* **5**, 112–119.

Kaoui, B., Ristow, G., Cantat, I., Misbah, C. & Zimmermann, W. 2008 Lateral migration of a two-dimensional vesicle in unbounded Poiseuille flow. *Phys. Rev.* E **77**, 021903.

Kersaudy-Kerhoas, M., Dhariwal, R., Desmulliez, M. P. Y. & Jouvet, L. 2010 Hydrodynamic blood plasma separation in microfluidic channels. *Microfluid Nanofluid* **8**, 105–114.

Kim, Y. W. & Yoo, J. Y. 2008 The lateral migration of neutrally-buoyant spheres transported through square microchannels. *J. Micromech. Microengng* **18**, 065015.

Lefebvre, A. 2007 Fluid–particle simulations with FreeFem++. In *ESAIM: Proc.*, vol. 18, pp. 120–132. ESAIM.

Maury, B. 2009 Numerical analysis of a finite element/volume penalty method. *SIAM J. Numer. Anal.* **47** (2), 1126–1148.

Mayrovitz, H. N. & Roy, J. 1983 Microvascular blood flow: evidence indicating a cubic dependence on arteriolar diameter. *Am. J. Physiol.* **255**, H1031–H1038.

McWhirter, J. L., Noguchi, H. & Gompper, G. 2009 Flow-induced clustering and alignment of vesicles and red blood cells in microcapillaries. *Proc. Natl Acad. Sci. USA* **106**, 6039–6043.

Mortazavi, S. & Tryggvason, G. 2000 A numerical study of the motion of drops in Poiseuille flow. Part 1. Lateral migration of one drop. *J. Fluid. Mech.* **411**, 325–350.

Noguchi, H. 2010 Dynamic modes of red blood cells in oscillatory shear flow. *Phys. Rev.* E **81**, 061920.

Obrist, D., Weber, B., Buck, A. & Jenny, P. 2010 Red blood cell distribution in simplified capillary networks. *Phil. Trans. R. Soc. Lond.* A **368**, 2897–2918.

Olla, P. 1997 The lift on a tank-treading ellipsoidal cell in a shear flow. *J. Phys.* II *Paris* **7**, 1533–1540.

Pamme, N. 2007 Continuous flow separations in microfluidic devices. *Lab Chip* **7**, 1644–1659.

Peyla, P. 2007 A deformable object in a microfluidic configuration: a numerical study. *Europhys. Lett.* **80**, 34001.

Podgorski, T., Callens, N., Minetti, C., Coupier, G., Dubois, F. & Misbah, C. 2010 Dynamics of vesicle suspensions in shear flow between walls. *Microgravity Sci. Technol.* **23**, 263–270.

Pries, A. R., Ley, K., Claassen, M. & Gaethgens, P. 1989 Red cell distribution at microvascular bifurcations. *Microvasc. Res.* **38**, 81–101.

Pries, A. R., Secomb, T. W. & Gaethgens, P. 1996 Biophysical aspects of blood flow in the microvasculature. *Cardiovasc. Res.* **32**, 654–667.

Risso, F., Collé-Paillot, F. & Zagzoule, M. 2006 Experimental investigation of a bioartificial capsule flowing in a narrow tube. *J. Fluid. Mech.* **547**, 149–173.

Roberts, B. W. & Olbricht, W. L. 2003 Flow-induced particulate separations. *AIChE J.* **49**, 2842–2849.

Roberts, B. W. & Olbricht, W. L. 2006 The distribution of freely suspended particles at microfluidic bifurcations. *AIChE J.* **52**, 199–206.

Schindler, M. & Ajdari, A. 2008 Droplet traffic in microfluidic networks: a simple model for understanding and designing. *Phys. Rev. Lett.* **100**, 044501.

Schonberg, J. A. & Hinch, E. J. 1989 Inertial migration of a sphere in a Poiseuille flow. *J. Fluid Mech.* **203**, 517–524.

Secomb, T. W., Styp-Rekowska, B. & Pries, A. R. 2007 Two-dimensional simulation of red blood cell deformation and lateral migration in microvessels. *Ann. Biomed. Engng* **35**, 755–765.

Sessoms, D. A., Belloul, M., Engl, W., Roche, M., Courbin, L. & Panizza, P. 2009 Droplet motion in microfluidic networks: hydrodynamic interactions and pressure-drop measurements. *Phys. Rev.* E **80**, 016317.

Svanes, K. & Zweifach, B. W. 1968 Variations in small blood vessel hematocrits produced in hypothermic rats by micro-occlusion. *Microvasc. Res.* **1**, 210–220.

Tanaka, H. & Araki, T. 2000 Simulation method of colloidal suspensions with hydrodynamic interactions: fluid particle dynamics. *Phys. Rev. Lett.* **85** (6), 1338–1341.

Vitkova, V., Mader, M.-A., Polack, B., Misbah, C. & Podgorski, T. 2008 Micro–macro link in rheology of erythrocyte and vesicle suspensions. *Biophys. J.* **95**, 33–35.

Vlahovska, P. M., Podgorski, T. & Misbah, C. 2009 Vesicles and red blood cells in flow: from individual dynamics to rheology. *C. R. Physique* **10**, 775–789.

White, F. M. 1991 *Viscous Fluid Flow*. McGraw-Hill.

Yang, S., Ündar, A. & Zahn, J. D. 2006 A microfluidic device for continuous, real time blood plasma separation. *Lab Chip* **6**, 871–880.

Yang, S. & Zahn, J. D. 2004 Particle separation in microfluidic channels using flow rate control. In *Proc. ASME Conf. International Mechanical Engineering Exp Fluids Engineering (IMECE)*, Anaheim, CA.

Yen, R. T. & Fung, Y. C. 1978 Effect of velocity distribution on red cell distribution in capillary blood vessels. *Am. J. Physiol. Heart Circ. Physiol.* **235**, H251–H257.

Yoo, J. Y. & Kim, Y. W. 2010 Two-phase flow laden with spherical particles in a microcapillary. *Intl J. Multiphase Flow* **36**, 460–466.

Zheng, S., Liu, J.-Q. & Tai, Y.-C. 2008 Streamline-based microfluidic devices for erythrocytes and leukocytes separation. *J. Microelectromech. Syst.* **17**, 1029–1038.